Supporting Information

Investigation of the Inhibition Mechanism of Xanthine Oxidoreductase by Oxipurinol: A Computational Study

Yazdan Maghsoud,[1] Chao Dong,[2] and G. Andrés Cisneros*[,1,3]

[1]*Department of Chemistry and Biochemistry, The University of Texas at Dallas, Richardson, TX 75080, USA*

[2]*Department of Chemistry and Physics, The University of Texas Permian Basin, Odessa, TX 79762, USA*

[3]*Department of Physics, The University of Texas at Dallas, Richardson, TX 75080, USA*

*E-mail: andres@utdallas.edu

Contents

1. Refinement of the Bovine Milk XO–Oxipurinol Crystal Structure

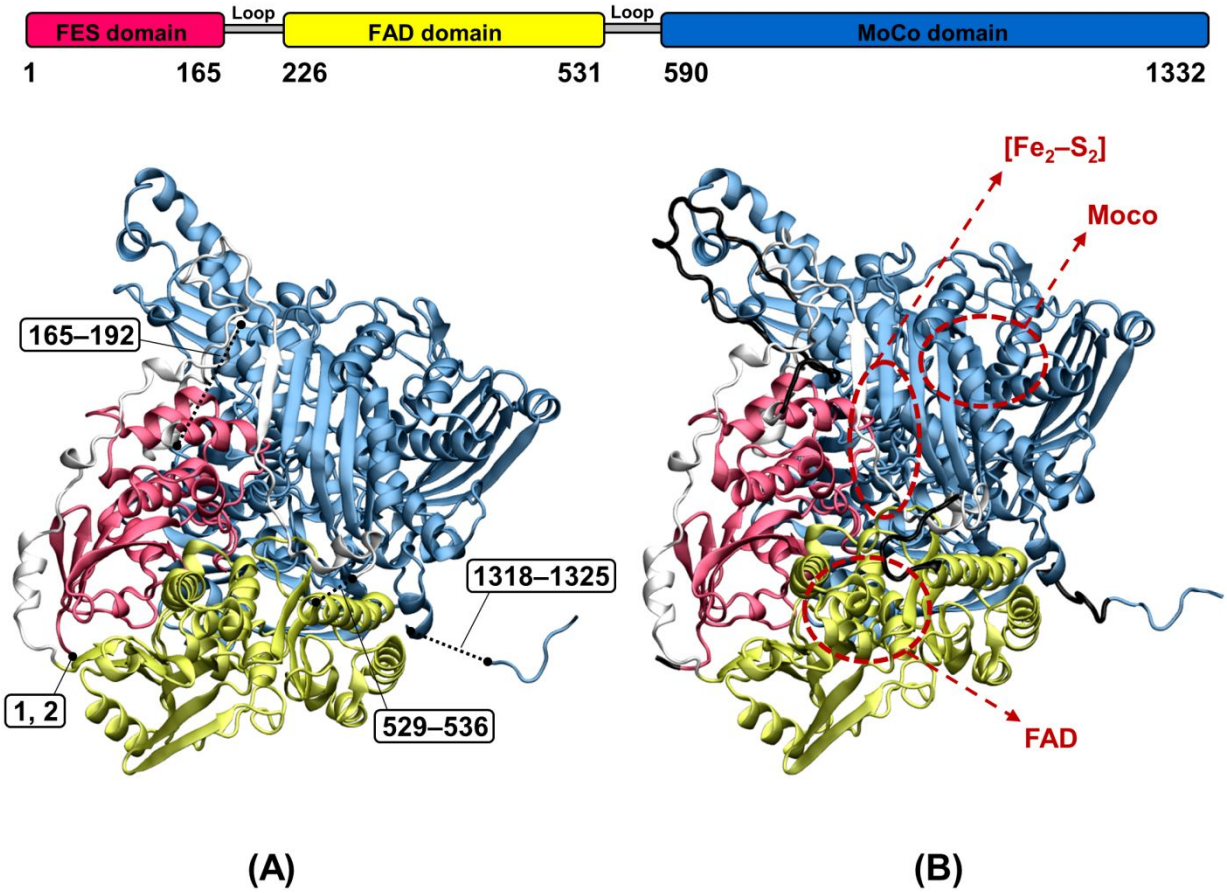

Figure S1. (A) The crystal structure of xanthine oxidase in complex with oxipurinol (PDB ID: 3BDJ) and its missing residues (1, 2, 165–192, 529–536, and 1318–1325). Missing residues are shown with corresponding residue numbers in dashed lines. **(B)** The modeled structure for XO–oxipurinol via MODELLER 10.1 and assessed by CASP and CAMEO. Modeled residues are shown in black ribbons.

After constructing the target-template alignment for 3BDJ, three-dimensional models of the target were calculated by using `automodel` class of MODELLER. Seven different models of XO were generated via the `model-single.py` script based on the 3BDJ. It is worth mentioning that the number of generated models are arbitrary; however, generating five to seven models is sufficient (see Ref. 127 of the manuscript). The best model can be selected by picking the one with the lowest value of the DOPE or SOAP assessment scores (lowest value means mostly negative). Herein, the DOPE assessment score was used for the evaluation. Based on this assessment, the third generated structures (3BDJ_1.B99990003.pdb) was the best and was selected for further MD simulations (see model-single.log file in the ESI). The PDB files of all the MODELLER-generated structures (3BDJ_1.B99990001.pdb to 3BDJ_1.B99990007.pdb) as well as the assessment scores are provided in the ESI (ESI-1.zip).

2. Parameterized Structures of the Non-Standard Residues

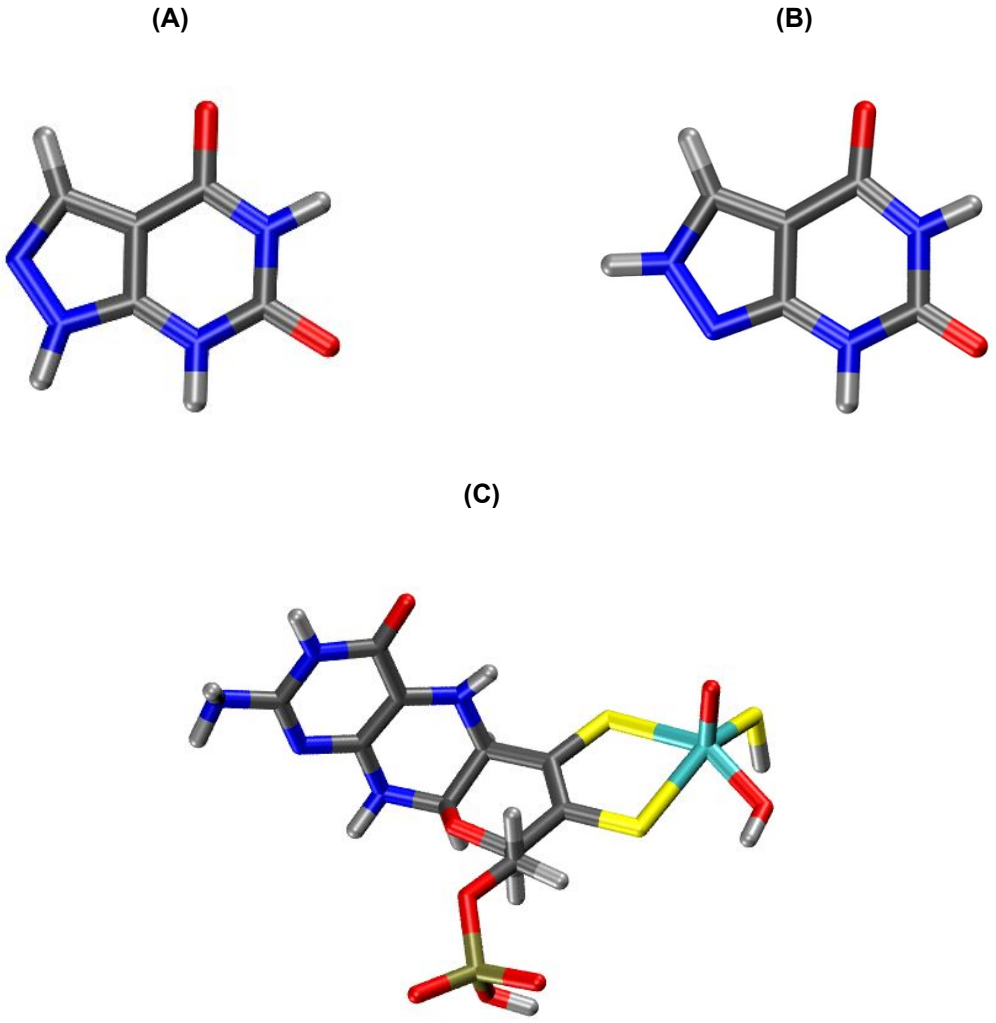

Figure S2. Parameterized structures for **(A)** oxipurinol (OXI), **(B)** tautomer-2 (OXI^{T-2}), and **(C)** reduced molybdenum cofactor.

3. Structural Analysis

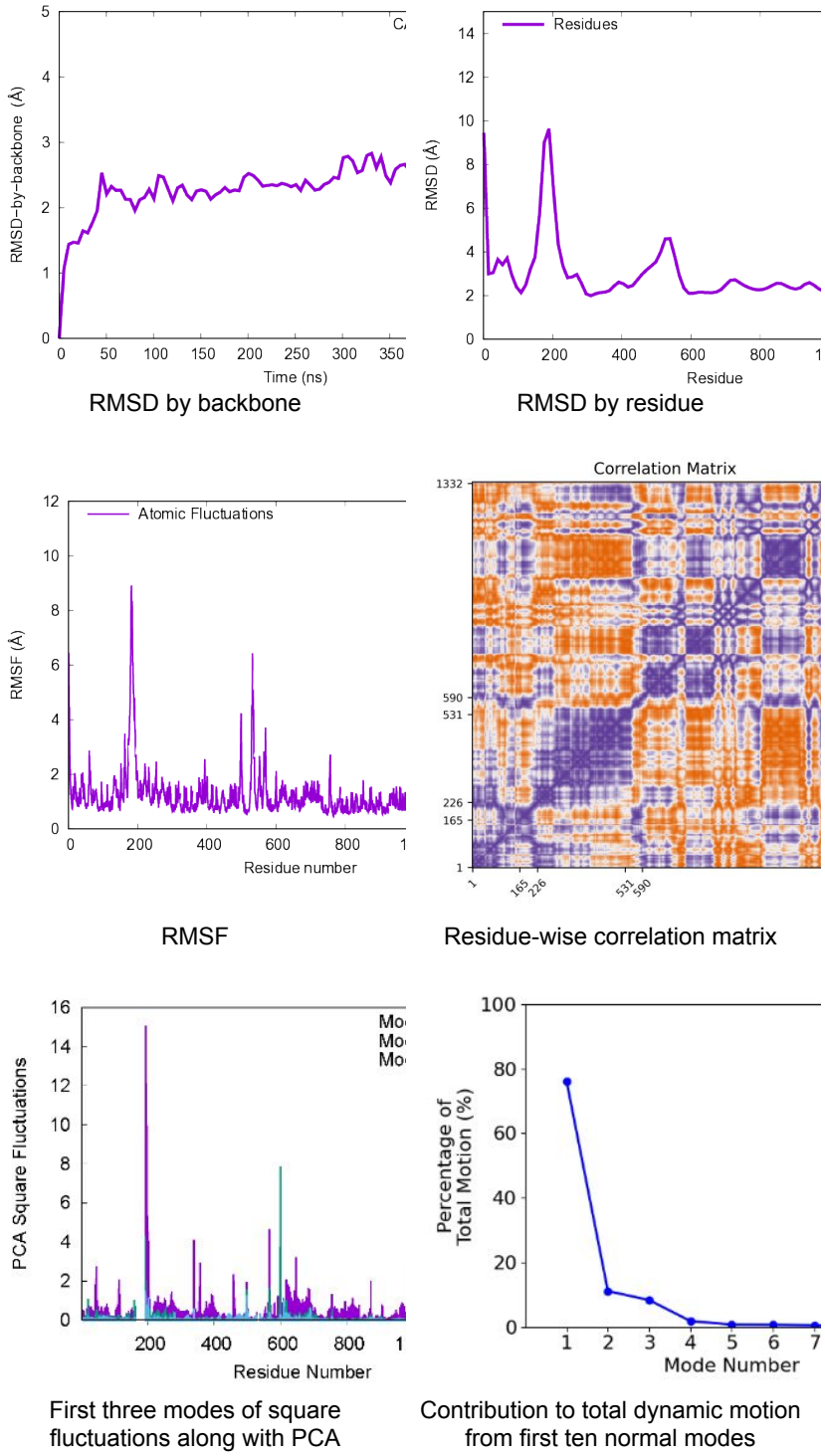

Figure S3. Structural analysis results for the MD simulation of the first replicate of the apo-XO. Areas of *correlation* in the residue-wise correlation matrix graph are blue (1.0), areas with *no correlation* are pale yellow (0.0), and areas with *anti-correlation* are red (–1.0).

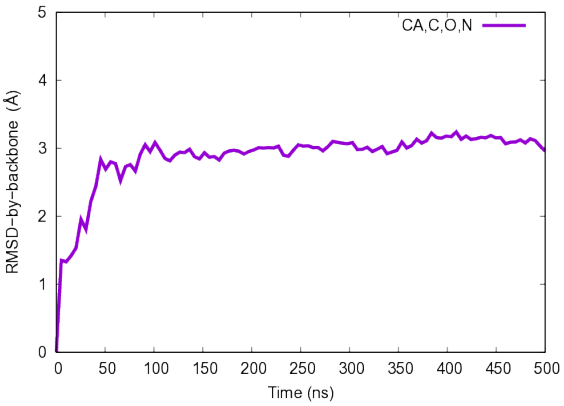

RMSD by backbone

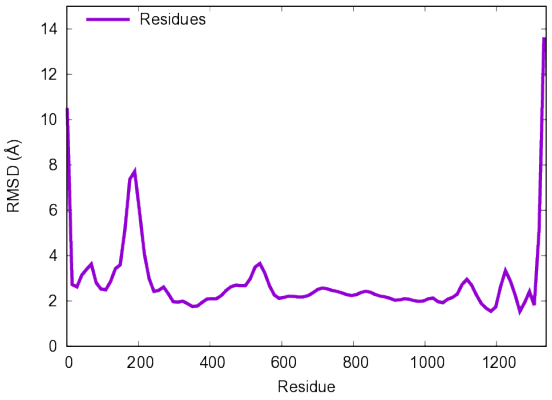

RMSD by residue

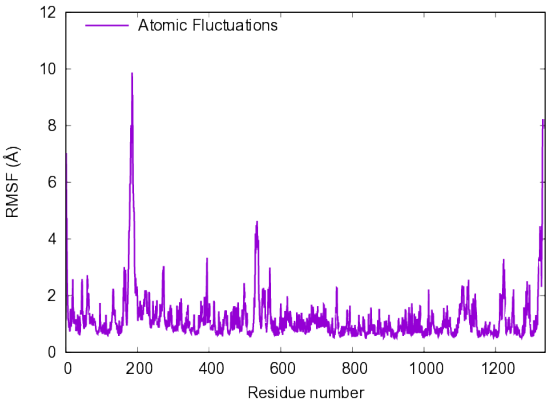

RMSF

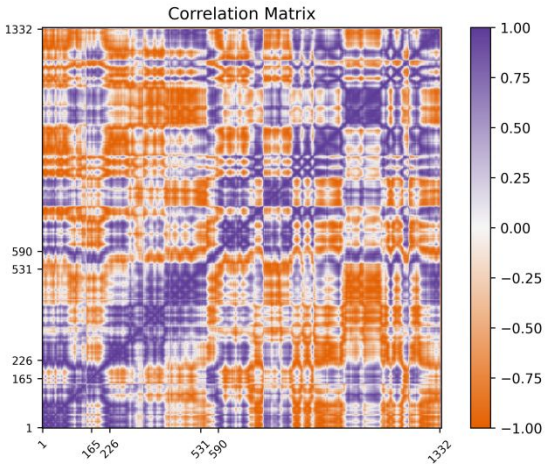

Residue-wise correlation matrix

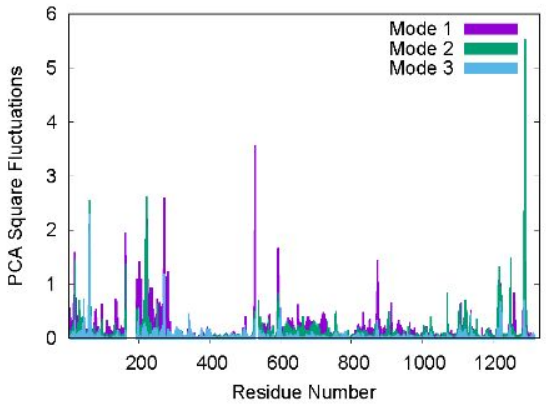

First three modes of square fluctuations along with PCA

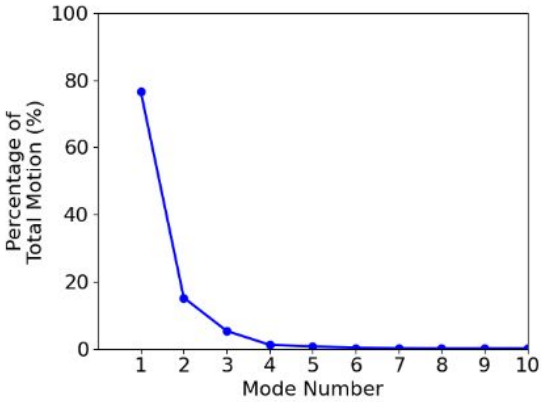

Contribution to total dynamic motion from first ten normal modes

Figure S4. Structural analysis results for the MD simulation of the second replicate of the apo-XO. Areas of *correlation* in the residue-wise correlation matrix graph are blue (1.0), areas with *no correlation* are pale yellow (0.0), and areas with *anti-correlation* are red (–1.0).

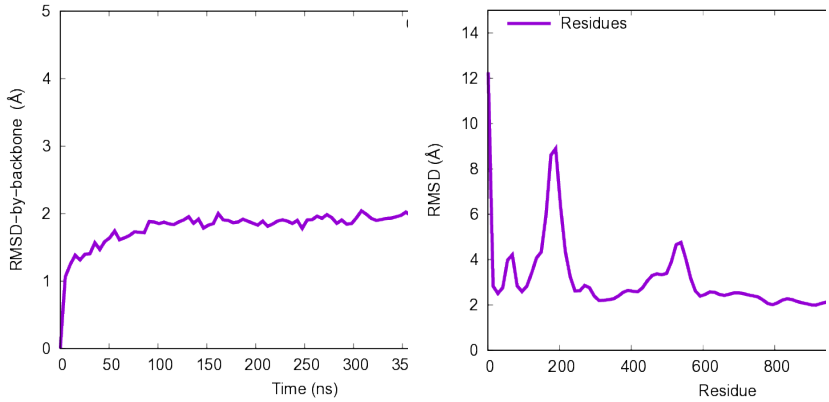

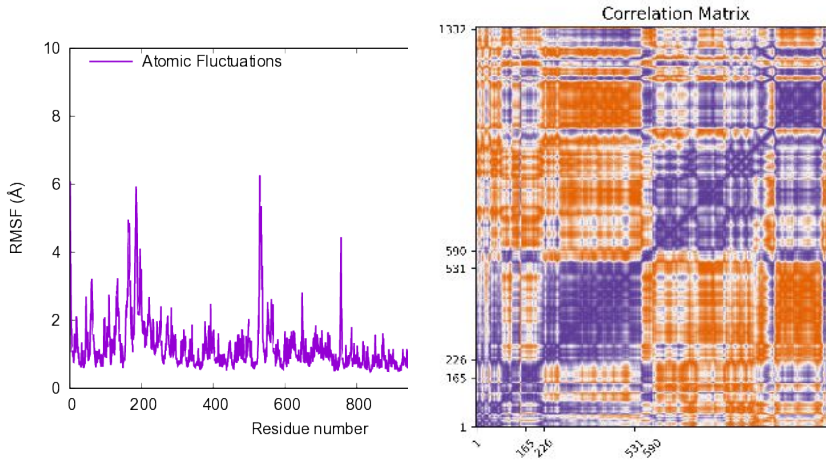

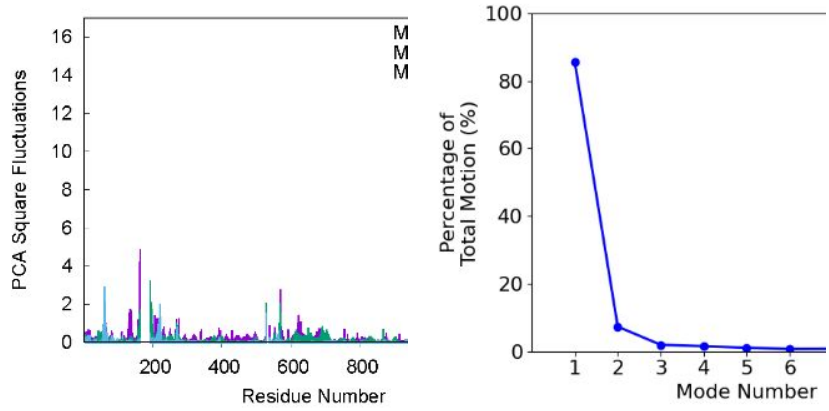

Figure S5. Structural analysis results for the MD simulation of the third replicate of the apo-XO. Areas of *correlation* in the residue-wise correlation matrix graph are blue (1.0), areas with *no correlation* are pale yellow (0.0), and areas with *anti-correlation* are red (–1.0).

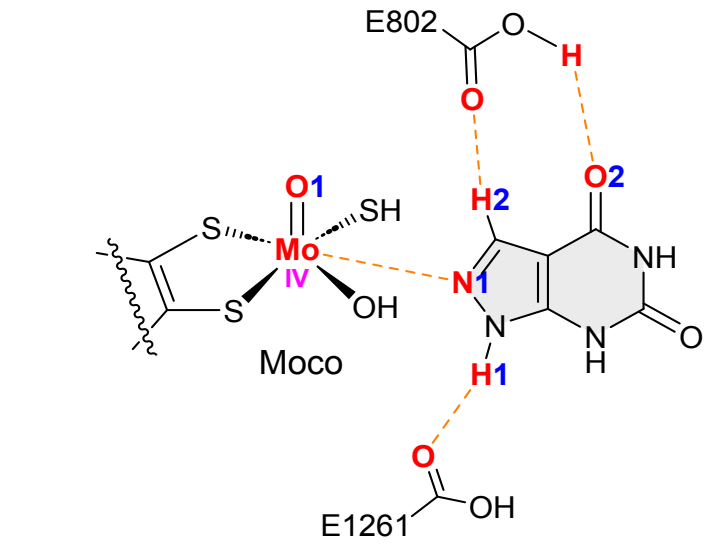

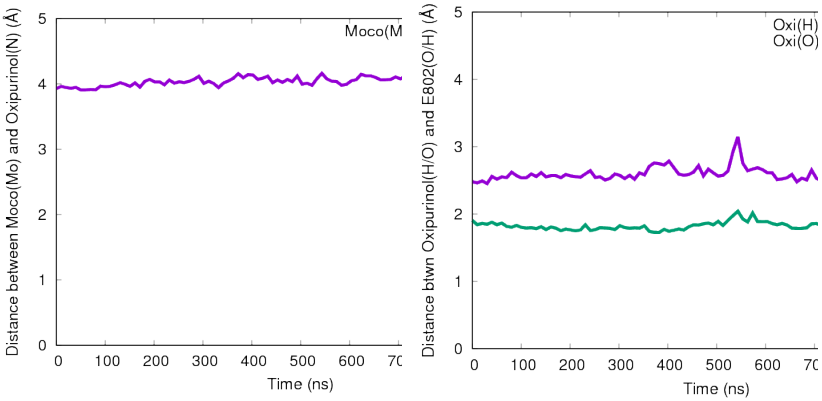

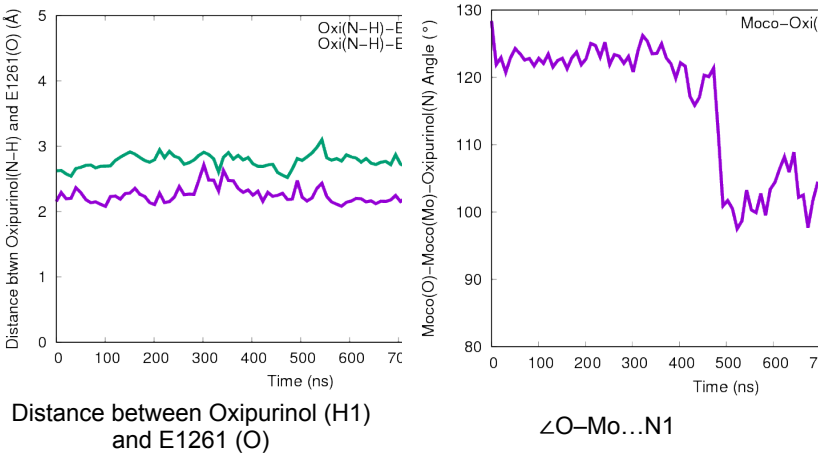

Figure S6. Structural analysis results for the MD simulation of the first replicate of the XO–OXI. Areas of *correlation* in the residue-wise correlation matrix graph are blue (1.0), areas with *no correlation* are pale yellow (0.0), and areas with *anti-correlation* are red (–1.0).

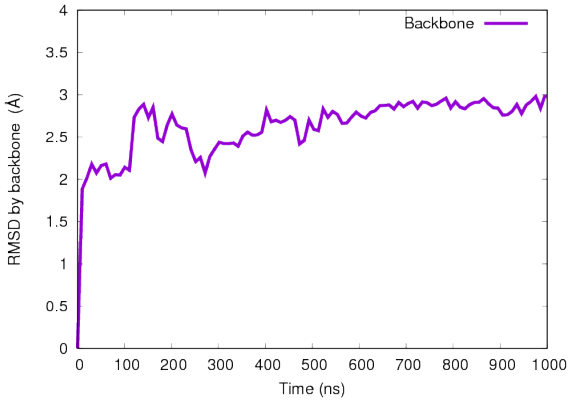

RMSD by backbone

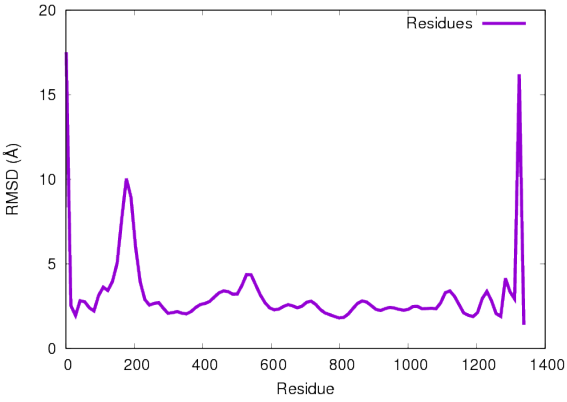

RMSD by residue

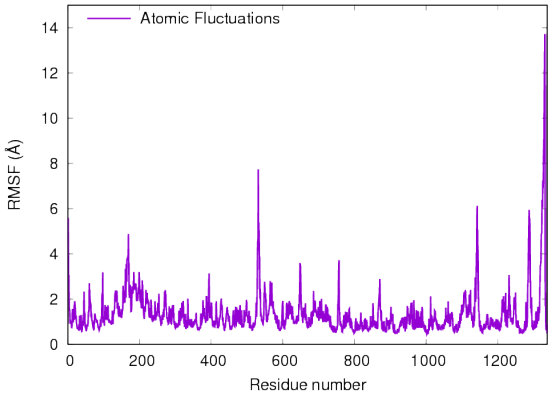

RMSF

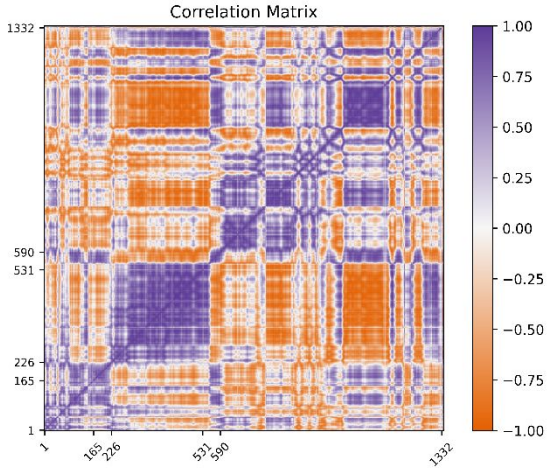

Residue-wise correlation matrix

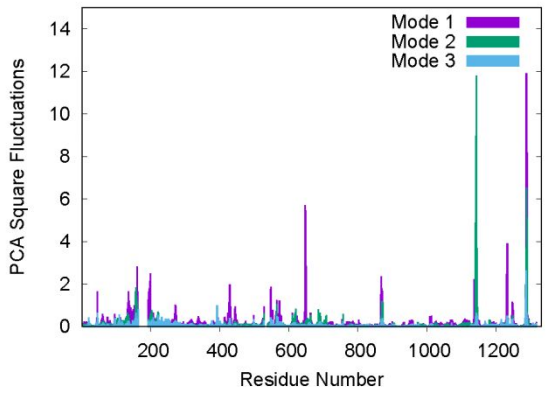

First three modes of square fluctuations along with PCA

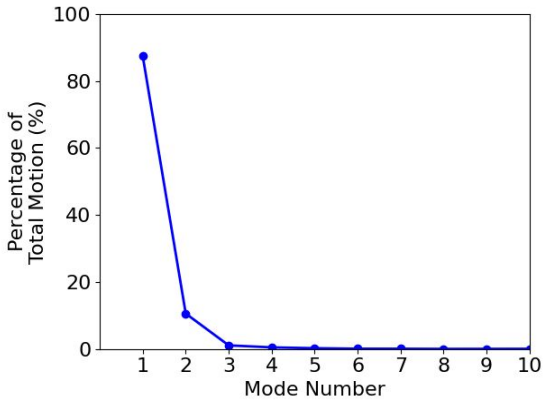

Contribution to total dynamic motion from first ten normal modes

Figure S6. Continued.

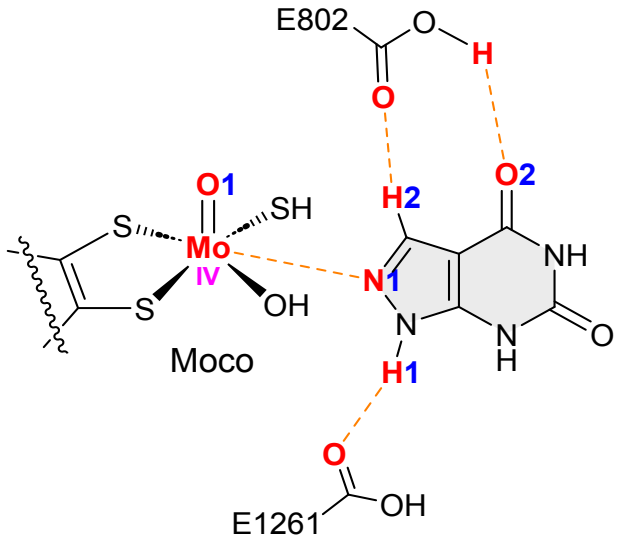

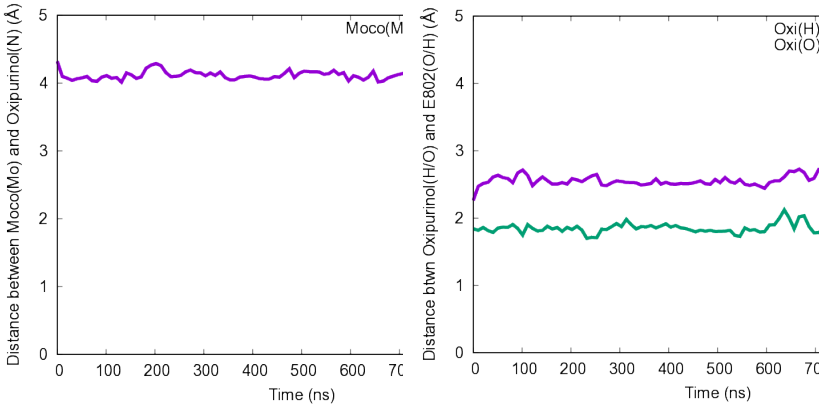

Distance between MoCo (Mo) and Oxipurinol (N1)

Distance between Oxipurinol (H2/O2) and E802 (O/H)

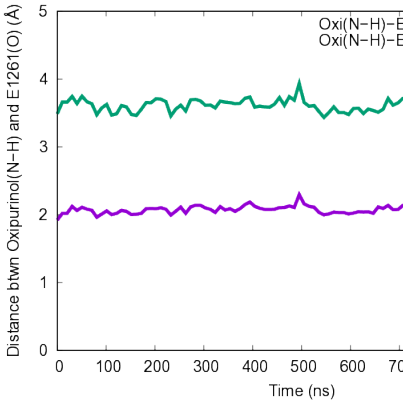

Distance between Oxipurinol (H1) and E1261 (O)

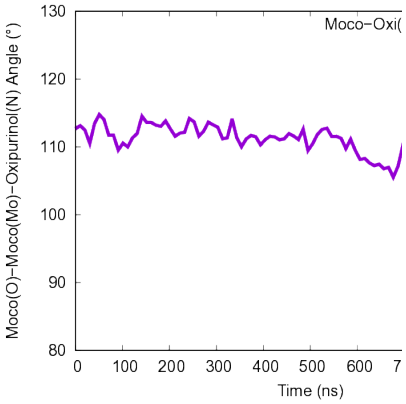

∠O–Mo…N1

Figure S7. Structural analysis results for the MD simulation of the second replicate of the XO–OXI. Areas of *correlation* in the residue-wise correlation matrix graph are blue (1.0), areas with *no correlation* are pale yellow (0.0), and areas with *anti-correlation* are red (–1.0).

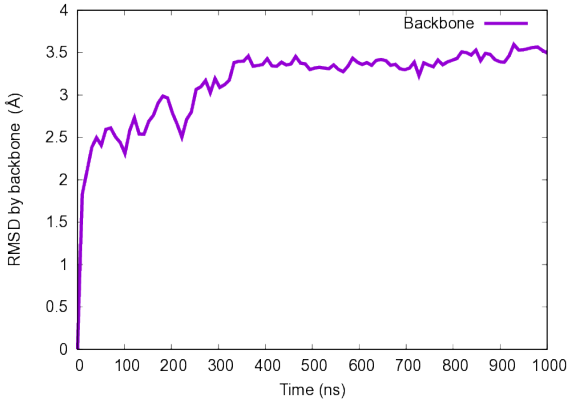

RMSD by backbone

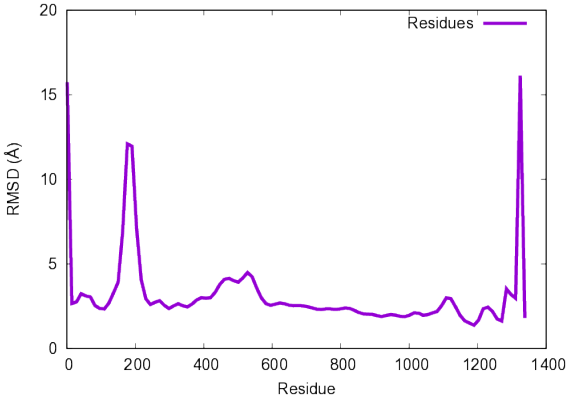

RMSD by residue

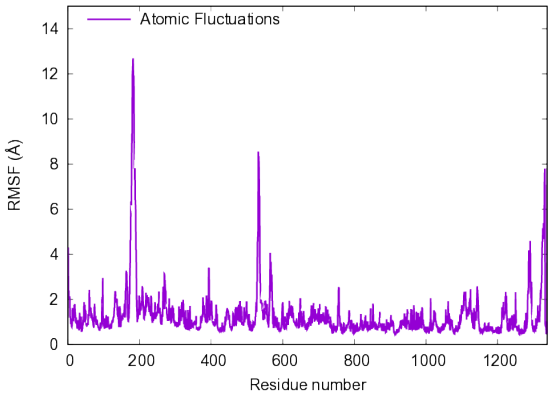

RMSF

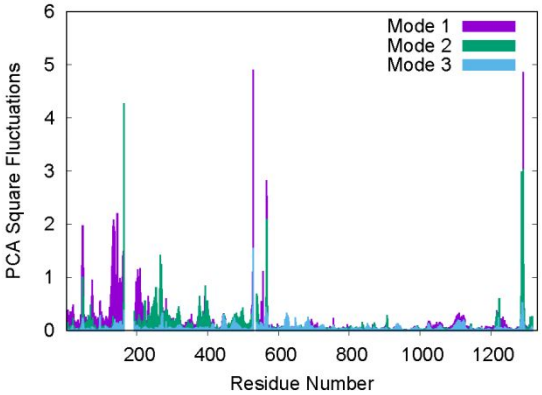

First three modes of square fluctuations along with PCA

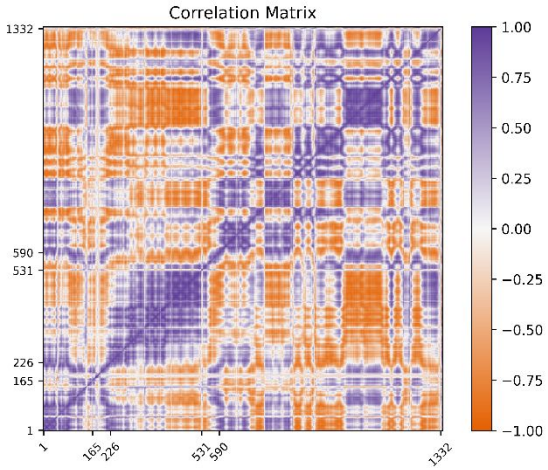

Residue-wise correlation matrix

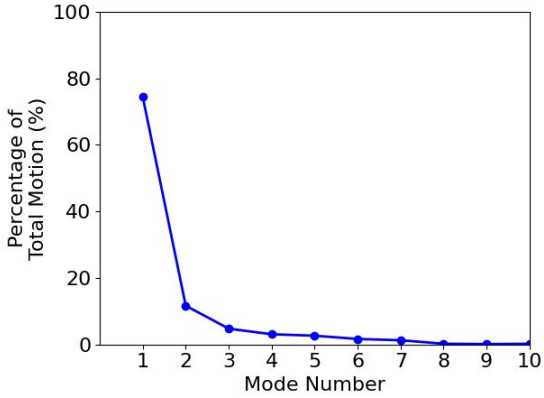

Contribution to total dynamic motion from first ten normal modes

Figure S7. Continued.

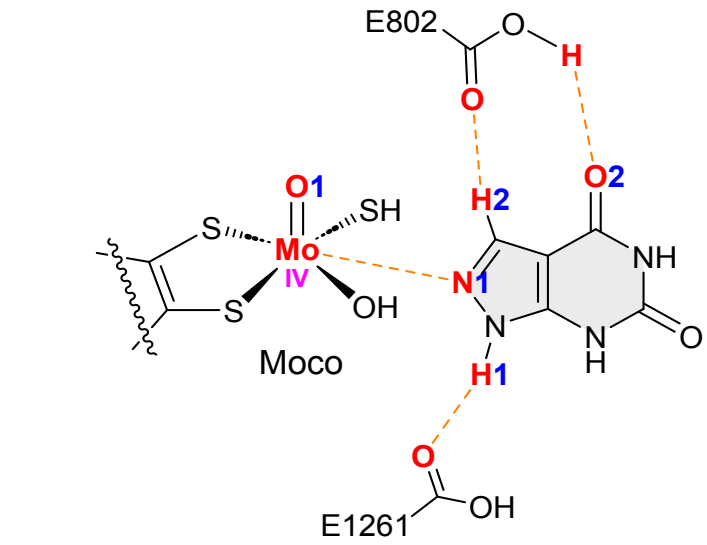

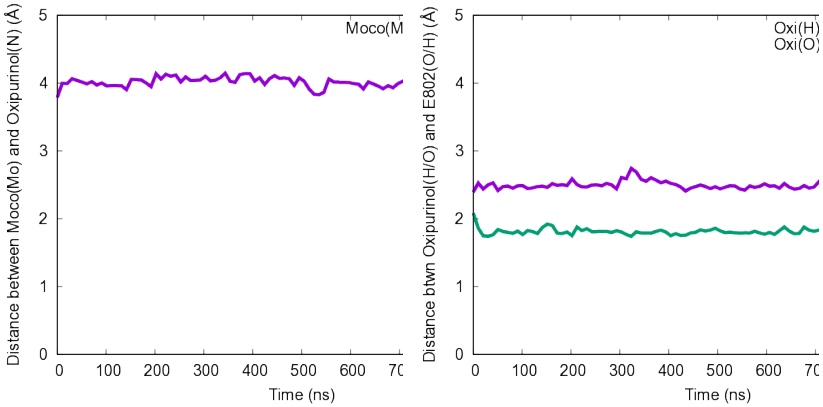

Distance between MoCo (Mo) and Oxipurinol (N1)

Distance between Oxipurinol (H2/O2) and E802 (O/H)

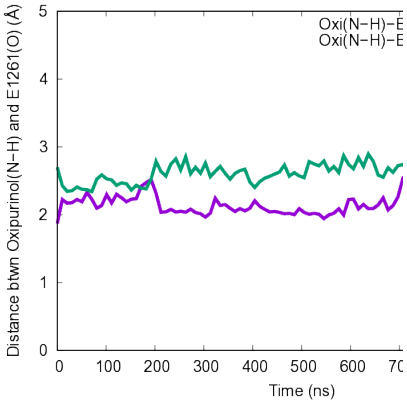

Distance between Oxipurinol (H1) and E1261 (O)

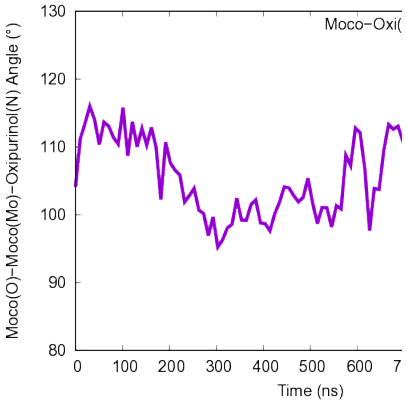

∠O–Mo…N1

Figure S8. Structural analysis results for the MD simulation of the third replicate of the XO–OXI. Areas of *correlation* in the residue-wise correlation matrix graph are blue (1.0), areas with *no correlation* are pale yellow (0.0), and areas with *anti-correlation* are red (–1.0).

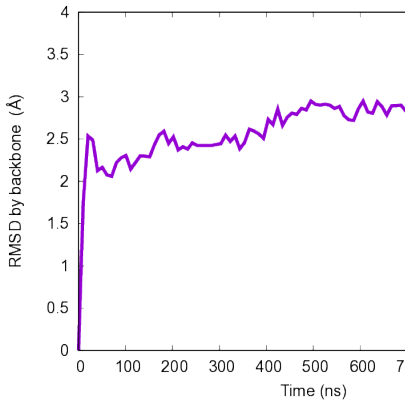

RMSD by backbone

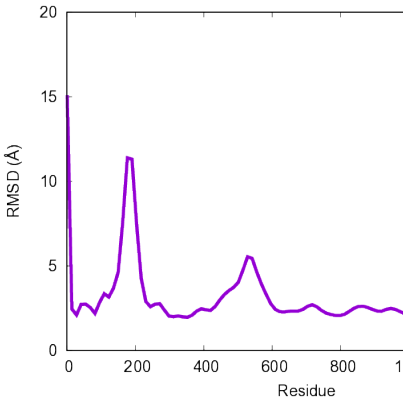

RMSD by residue

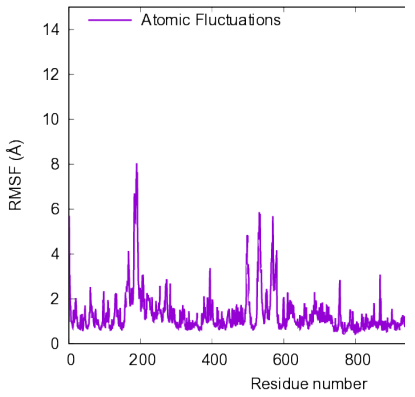

RMSF

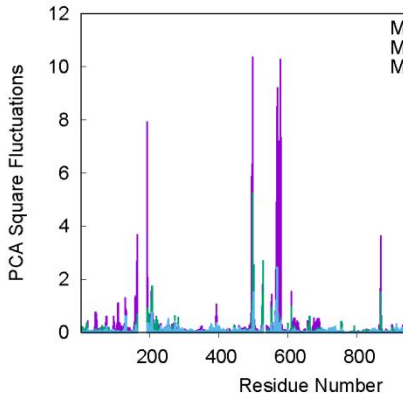

First three modes of square fluctuations along with PCA

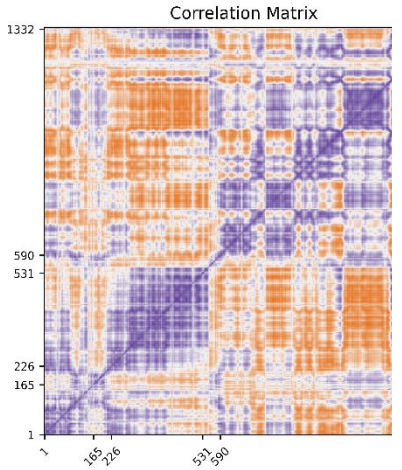

Residue-wise correlation matrix

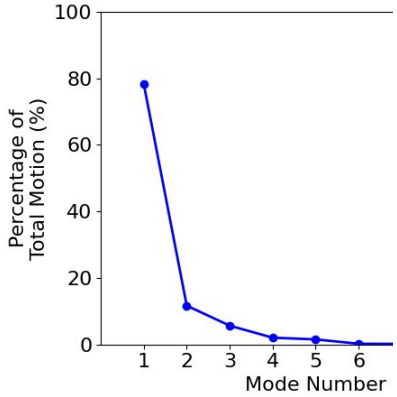

Contribution to total dynamic motion from first ten normal modes

Figure S8. Continued.

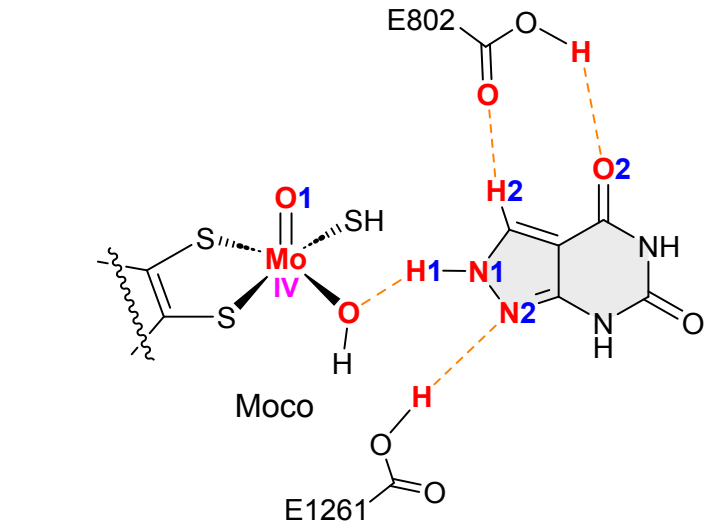

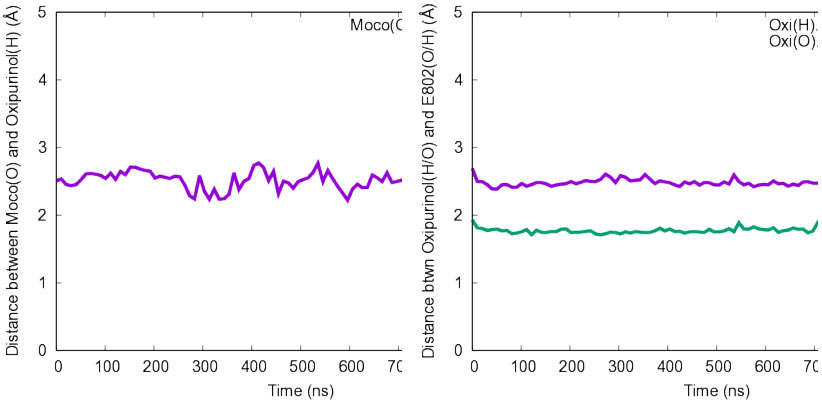

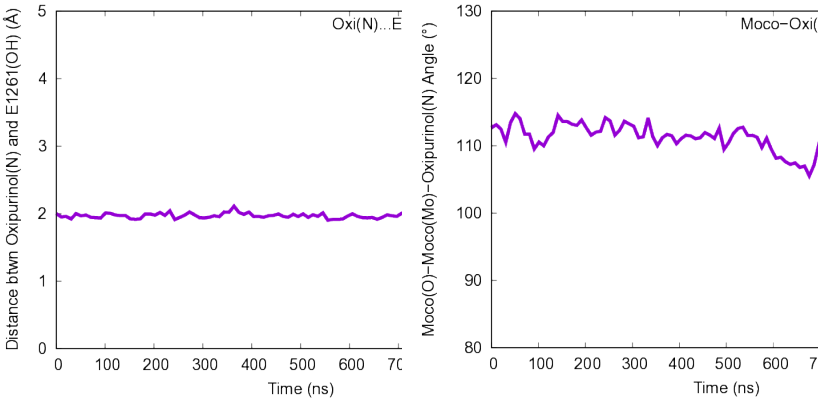

Figure S9. Structural analysis results for the MD simulation of the first replicate of the XO–OXI$^{T\text{-}2}$. Areas of *correlation* in the residue-wise correlation matrix graph are blue (1.0), areas with *no correlation* are pale yellow (0.0), and areas with *anti-correlation* are red (–1.0).

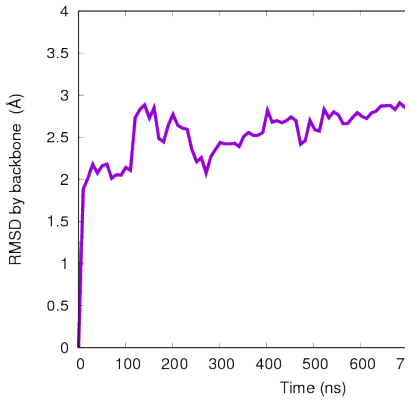

RMSD by backbone

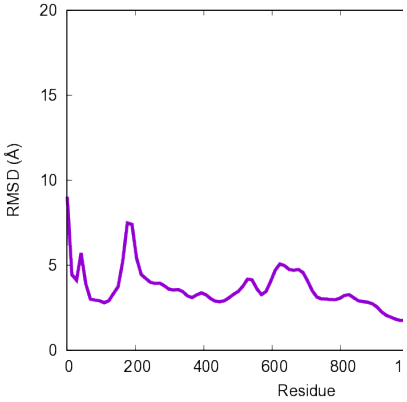

RMSD by residue

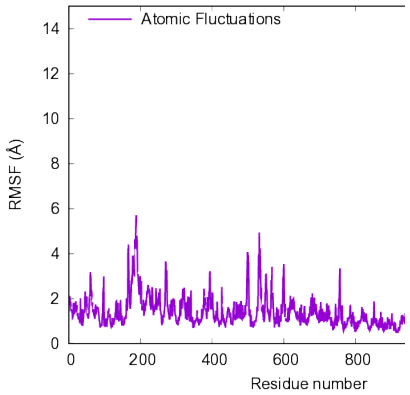

RMSF

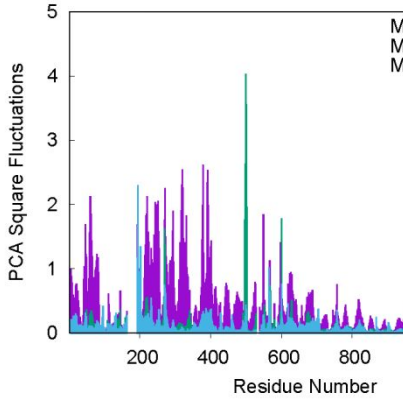

First three modes of square fluctuations along with PCA

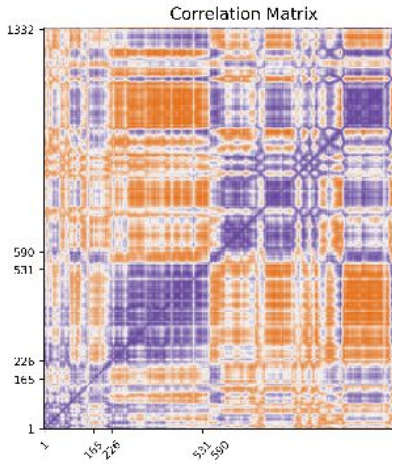

Residue-wise correlation matrix

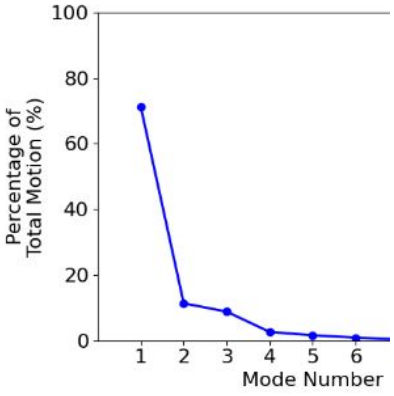

Contribution to total dynamic motion from first ten normal modes

Figure S9. Continued.

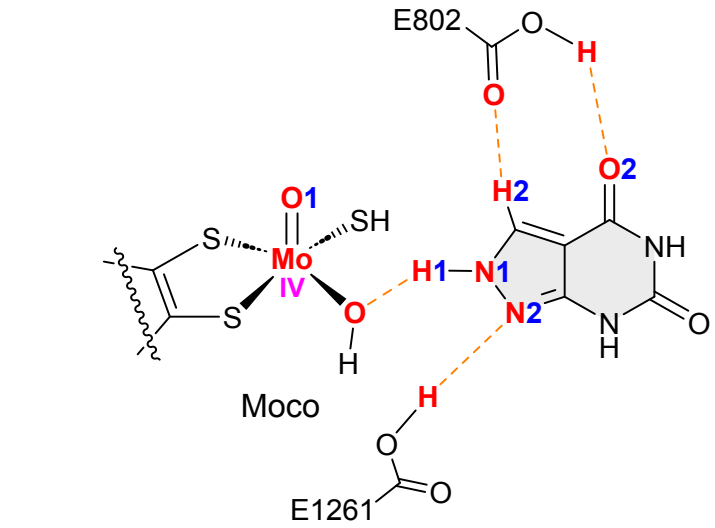

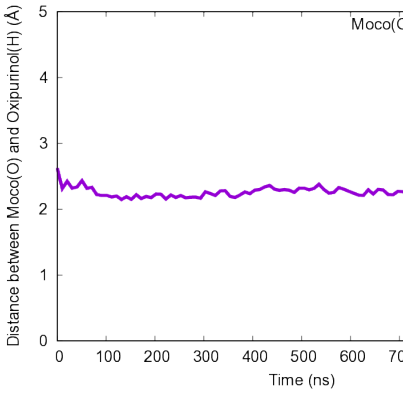

Distance between MoCo (O) and Oxipurinol (H1)

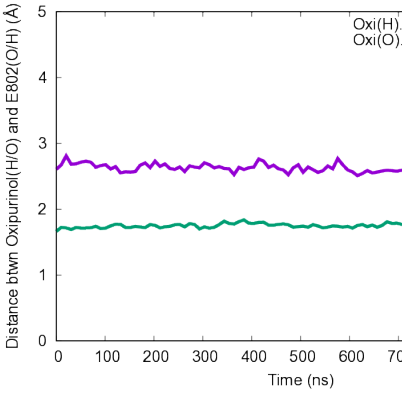

Distance between Oxipurinol (H2/O2) and E802 (O/H)

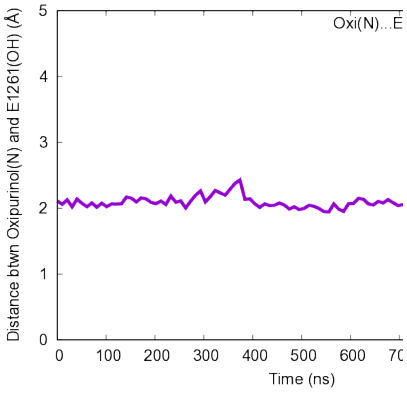

Distance between Oxipurinol (N2) and E1261 (H)

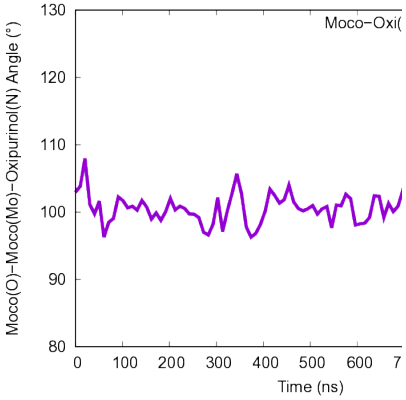

∠O–Mo…N1

Figure S10. Structural analysis results for the MD simulation of the second replicate of the XO–OXI$^{T\text{-}2}$. Areas of *correlation* in the residue-wise correlation matrix graph are blue (1.0), areas with *no correlation* are pale yellow (0.0), and areas with *anti-correlation* are red (–1.0).

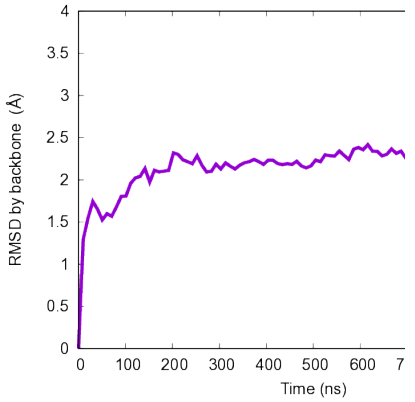

RMSD by backbone

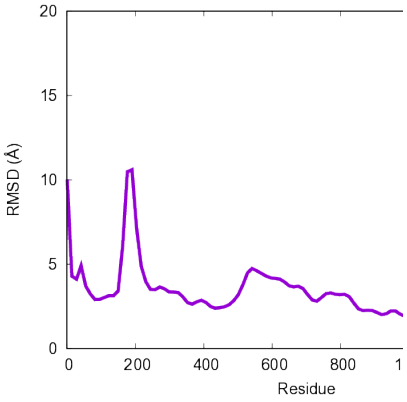

RMSD by residue

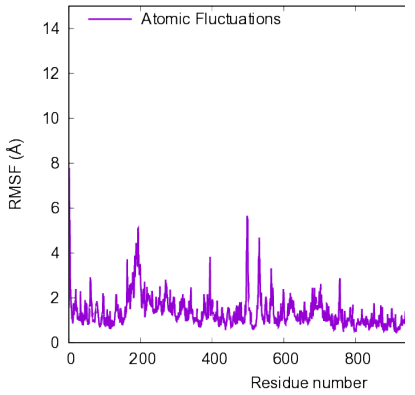

RMSF

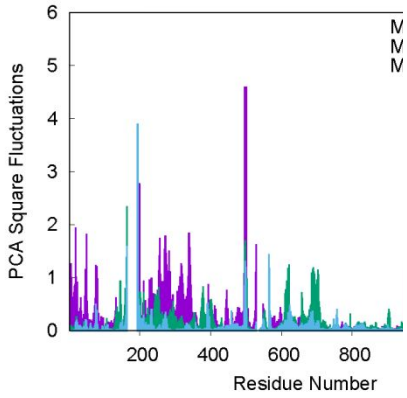

First three modes of square fluctuations along with PCA

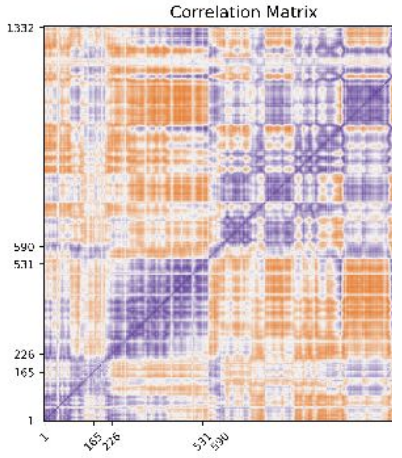

Residue-wise correlation matrix

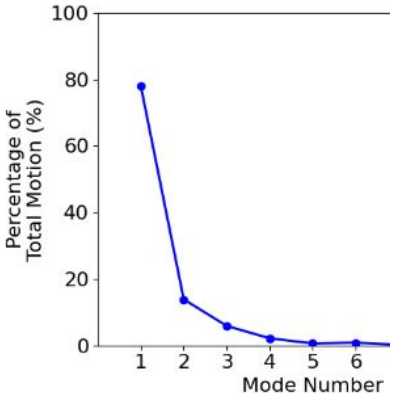

Contribution to total dynamic motion from first ten normal modes

Figure S10. Continued.

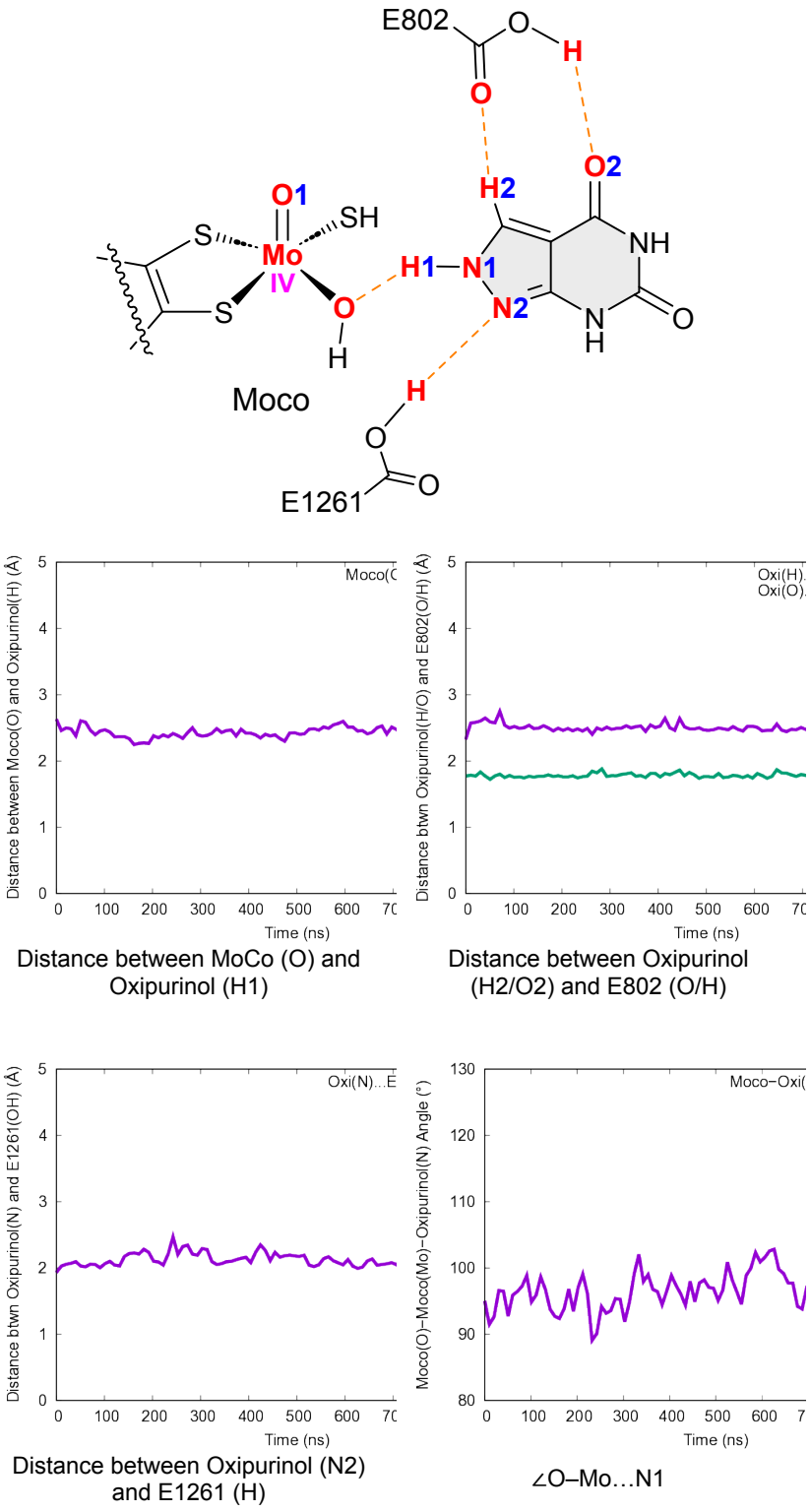

Figure S11. Structural analysis results for the MD simulation of the third replicate of the XO–OXI$^{T\text{-}2}$. Areas of *correlation* in the residue-wise correlation matrix graph are blue (1.0), areas with *no correlation* are pale yellow (0.0), and areas with *anti-correlation* are red (–1.0). More explanations are provided on the next page.

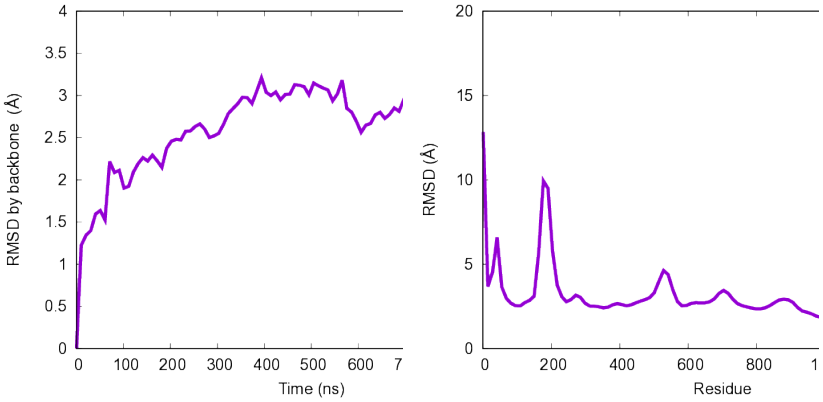

RMSD by backbone

RMSD by residue

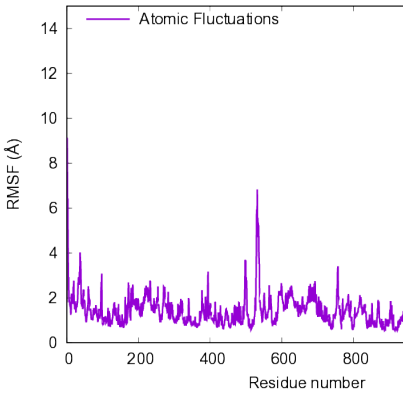

RMSF

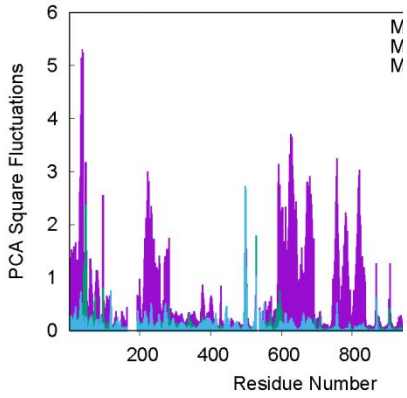

First three modes of square fluctuations along with PCA

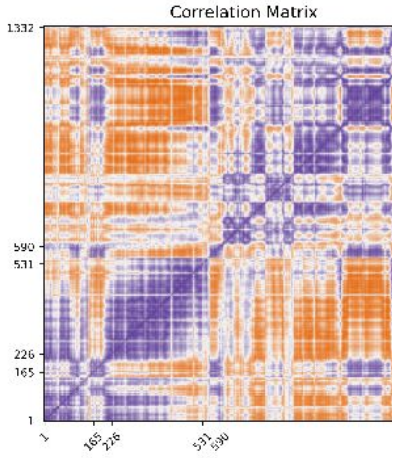

Residue-wise correlation matrix

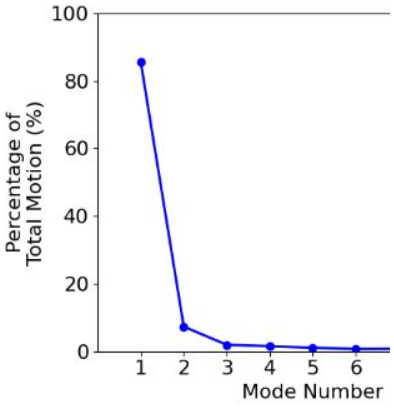

Contribution to total dynamic motion from first ten normal modes

Figure S11. Continued.

4. Clustering Analysis

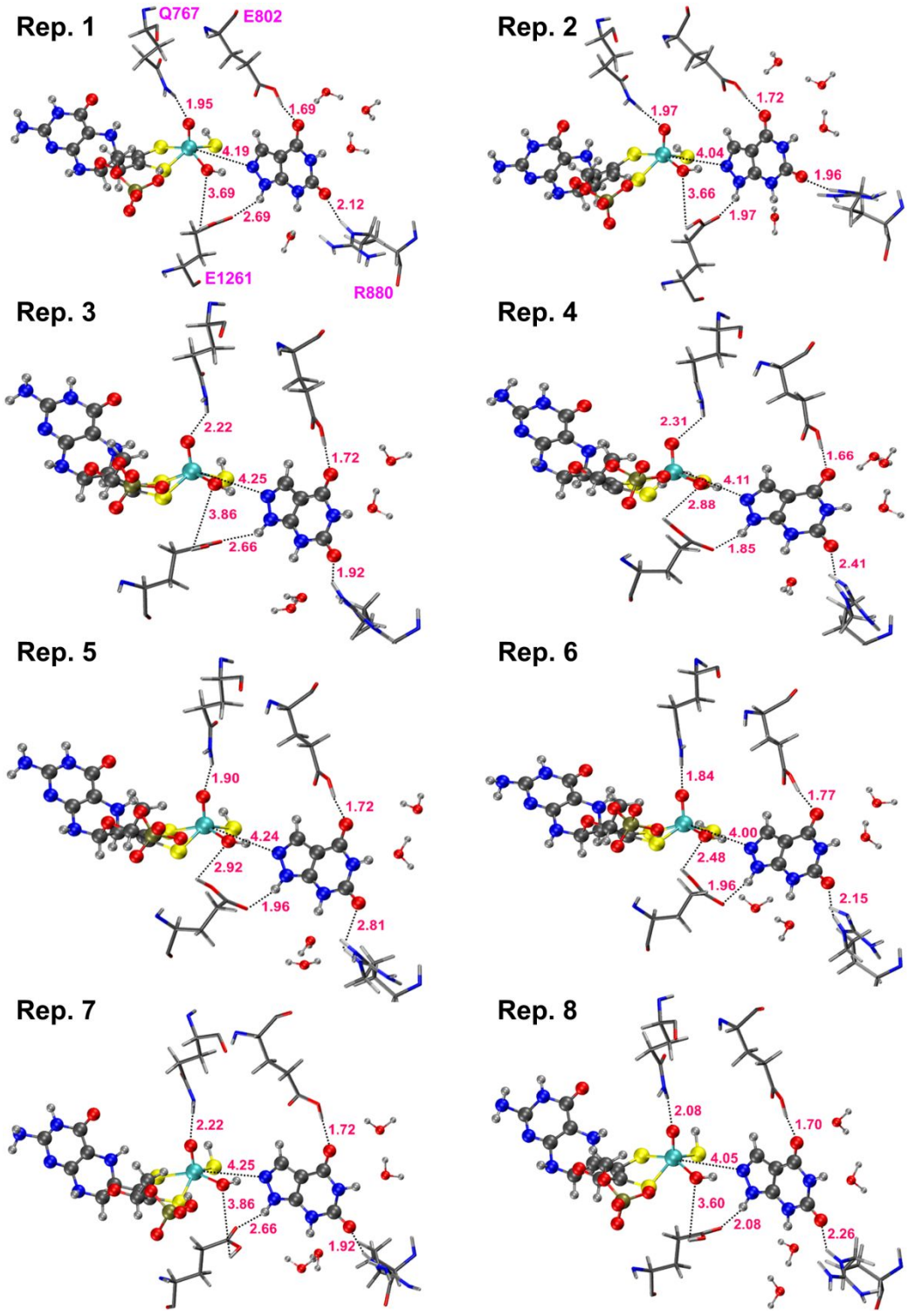

Figure S12. Selected frames from the clustering analysis and orientations of the active site residues in the XO–OXI bound system.

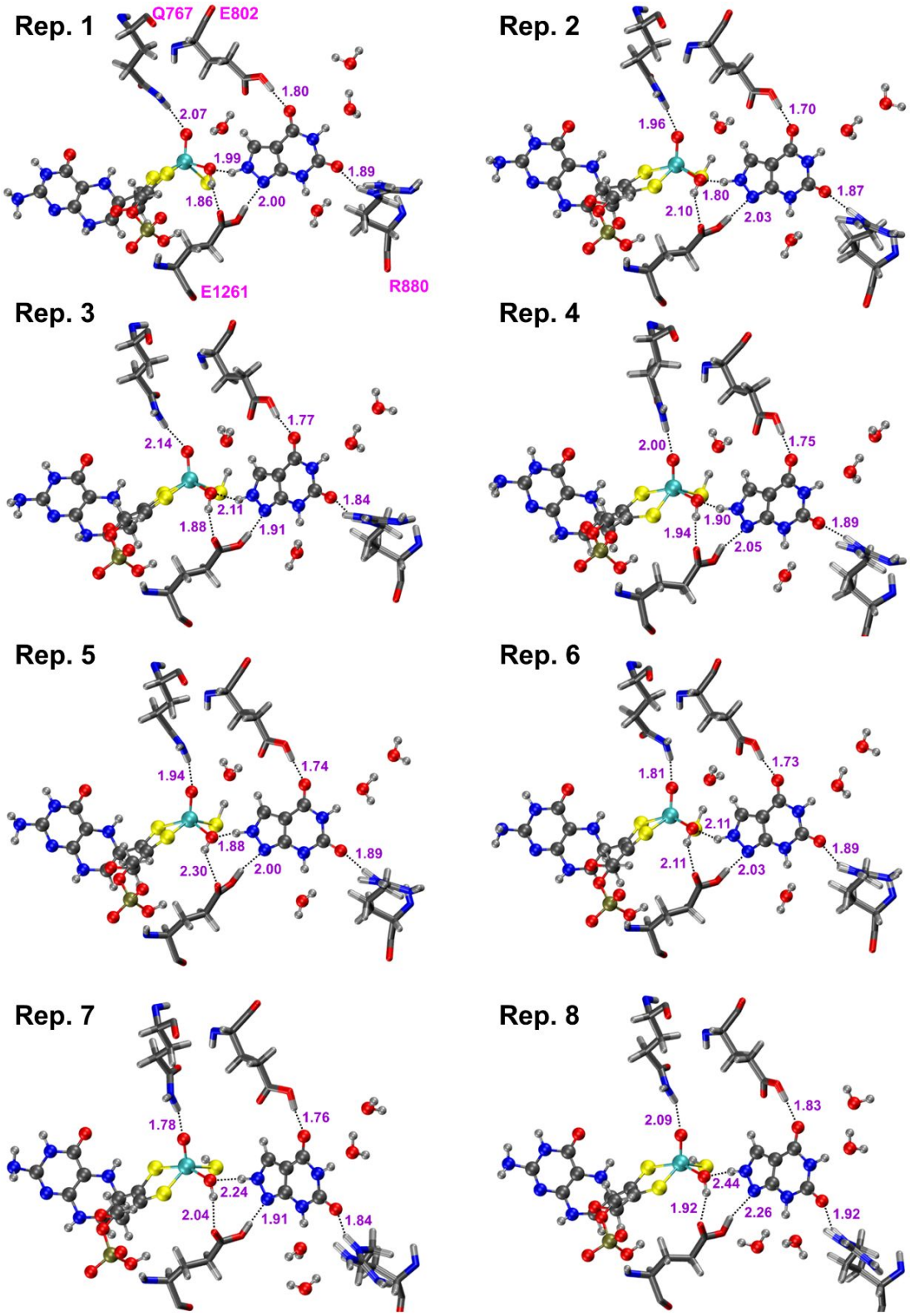

Figure S13. Selected frames from the clustering analysis and orientations of the active site residues in the XO–OXI^{T-2} bound system.

Table S1. Results of the *k*-means clustering and QM/MM optimization values for the selected representatives for XO–OXI systems. The QM/MM energies are calculated at the ωB97X-D/def2-SVP//ff14SB level of theory. Additional information and files can be found in the ESI (ESI-3.zip).

XO–OXI

Representative No.	Cluster No.	Frame No.	Abundance (%)	$E_{Relative}$ (kcal mol^{-1})
1	0	16317	17.1	344
2	1	88160	16.5	649
3	2	150161	12.9	476
4	1	190874	16.5	686
5	0	199718	17.1	386
6	0	236571	17.1	0
7	3	276558	10.7	155
8	1	285895	16.5	647

XO–OXI^{T-2}

Representative No.	Cluster No.	Frame No.	Abundance (%)	$E_{Relative}$ (kcal mol^{-1})
1	5	128697	9.1	734
2	2	128805	12.6	0
3	0	130301	16.7	710
4	2	160914	12.6	640
5	2	162636	12.6	789
6	5	190799	9.1	388
7	0	215942	16.7	463
8	3	260198	9.9	480

5. Components of the QM Subregion

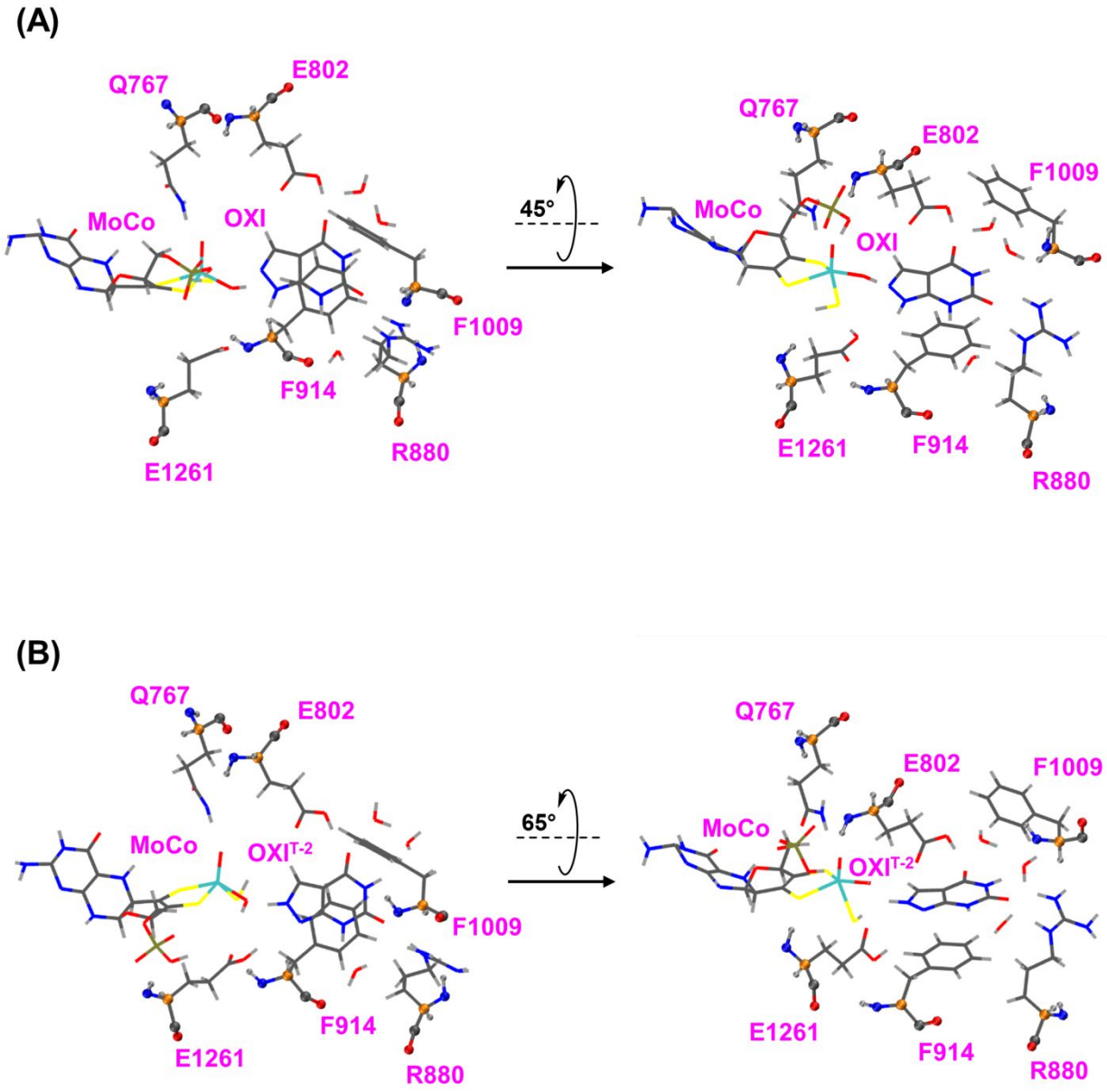

Figure S14. The QM subregion for **(A)** XO–OXI and **(B)** XO–OXI^{T-2}, which comprises 145 atoms, including the MoCo, oxipurinol, Q767, E802, R880, F914, F1009, E1261, and water molecules within 3 Å of the inhibitor. Two different view angles are provided for each structure for enhanced clarity. All the QM atoms are shown in the sticks, while the boundary atoms (H_α, C, O, N, and H) are shown in spheres and the C_α pseudobond atoms are in orange balls.

6. Oxipurinol Tautomers

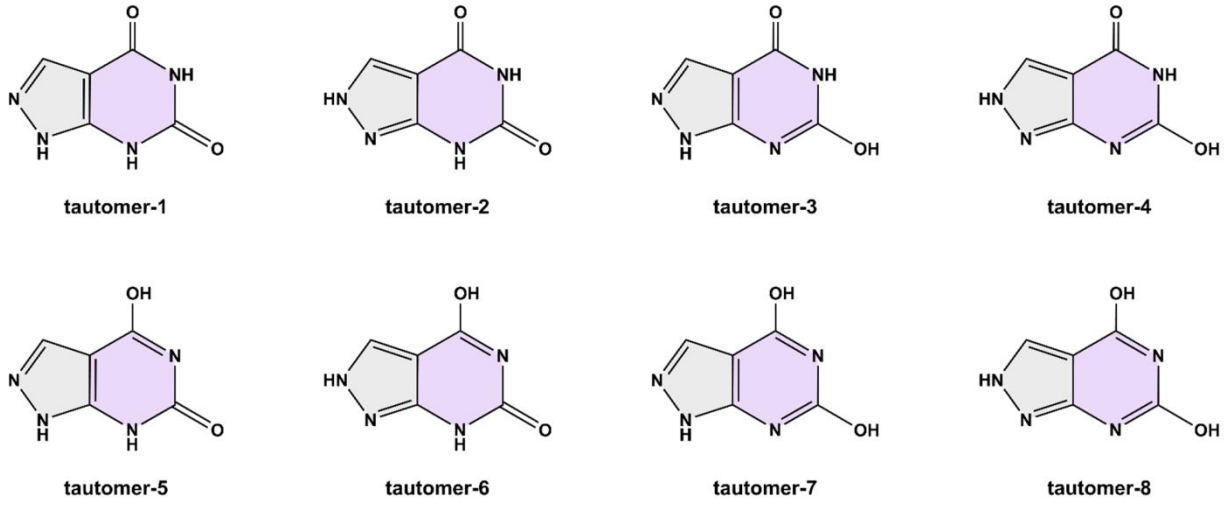

Figure S15. Schematics of eight tautomers of the neutral oxipurinol representing the di-keto, keto–enol, and di-enol forms. Plouvier and Choi [Ref. 197 in the manuscript] showed the probability of the existence of up to 38 tautomeric forms for the neutral oxipurinol; however, they noted that the functional derivative of this compound that possesses a biological activity (either functional or structural) is identical to tautomer-1.

7. EDA on the Pre-Catalytic Inhibition

Table S2. Residues with considerable non-bonded intermolecular interactions ($|\Delta E_{NB}| \geq 12.0$ kcal mol^{-1}) with the molybdenum cofactor of XO–OXI compared to apo-XO as the reference. The values of ΔE_{NB} (in kcal mol^{-1}) are calculated based on **Eq. 3** in the manuscript.

Stabilizing residues		Destabilizing residues	
Residue	ΔE_{NB}	Residue	ΔE_{NB}
R31	–16.8	E45	13.3
R32	–13.2	E89	13.2
R37	–12.0	E140	12.9
K40	–18.7	E428	13.5
R149	–19.7	D429	14.7
R154	–13.7	E562	12.5
K269	–12.8	D571	12.9
R426	–14.2	E589	12.9
R575	–13.4	D595	17.1
K771*	**–14.6**	**E652**	**12.4**
R790	–13.3	**D740**	**21.6**
K792	–15.9	E745	26.1
R793	–19.4	D828	14.7
K801	**–30.4**	E831	13.1
R804	**–14.3**	D832	21.1
R824	–13.2	**D872**	**14.1**
R829	–23.0	**E879**	**14.7**
R871	**–12.4**	D886	15.1
R880	**–18.4**	E924	14.2
R912	**–54.1**	E949	13.0
R942	–13.2	E960	14.6
R966	–13.4	E970	13.2
R980	–12.2	E1037	24.7
K1004	–18.7	E1065	15.7
K1045	–31.3	**D1084**	**21.7**
K1052	–15.5	D1177	14.0
S1080	**–20.1**	D1181	22.4
K1134	**–12.6**	D1191	30.2
R1175	–12.5	E1196	22.7
K1228	–12.4	E1209	22.5
R1240	–13.0	E1210	13.7
R1245	–12.9	E1238	12.6
K1250	–12.6	D1246	12.3
K1251	**–16.8**		
K1257	**–20.8**		

* Residues in bold text are located around the active site in the first- and second-shell of coordination.

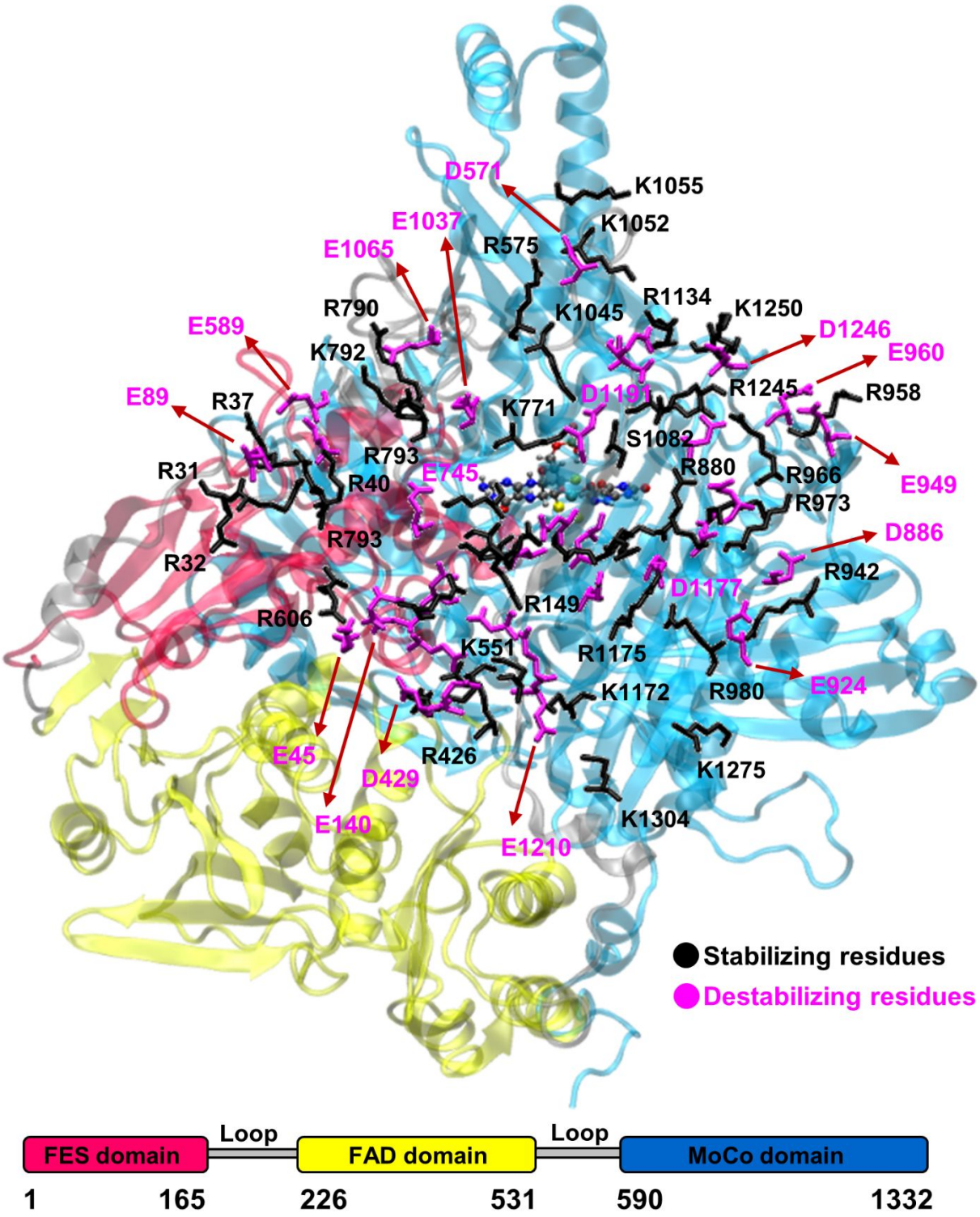

Table S2. Continued.

Table S3. Detailed list of the residues with stabilizing and destabilizing effects on the selected residues of the active site (MoCo, oxipurinol, and E1261) during the pre-catalytic inhibition of XO by oxipurinol.

Stabilizing residues		Destabilizing residues	
Residue	E_{NB}	Residue	E_{NB}
R31	–36.8	E45	35.3
R32	–38.5	E89	32.5
R37	–31.2	E103	33.5
K40	**–43.0**	E140	35.5
K95	–39.6	D141	30.8
R104	–31.0	E200	31.1
K107	–34.0	E428	36.3
R149[1]	**–69.5**	D429	36.1
R154	**–49.0**	D430	34.1
K269	–31.2	E562	36.3
R426	**–40.0**	E570	33.4
R427	–31.2	D571	37.4
K433	–31.1	E589	35.1
K551	–33.1	**D594**	**40.4**
R575	–36.9	**D595**	**41.3**
R606	**–35.2**	E602	32.5
K713	–33.3	E645	32.0
K716	–31.3	D651	41.2
K754	–32.0	**E652**	**45.6**
K771	**–53.9**	E679	31.7
K778	–36.5	E711	30.5
R790	–41.1	**D740**	**61.7**
K792	**–45.5**	**E745**	**73.0**
R793	**–55.9**	E761	35.4
K801	**–95.8**	D828	39.9
R804	**–54.1**	E831	38.2
R824	**–37.6**	**D832**	**60.4**
R829	**–57.3**	D862	31.5
R839	**–61.1**	**D872**	**51.8**
R871	**–49.7**	**E879**	**50.4**
R880	**–80.1**	**D886**	**43.1**
K890	–34.9	E924	39.8
R899	–31.2	E939	31.0
K902	–31.9	E949	35.5
R912	**–143.0**	D951	33.3
R942	–36.5	**E960**	**41.7**
R958	–32.9	D969	31.7
R966	–37.7	E970	35.7
K973	–32.9	**E1037**	**84.5**
R980	–33.6	**E1065**	**49.5**
K1004	**–49.3**	**D1084**	**73.5**
K1045	**–104.8**	E1092	38.0
K1052	**–42.1**	E1143	32.3
K1055	–30.8	D1177	38.0
K1060	–31.2	**D1181**	**56.3**
S1080	–38.4	**E1092**	**85.8**
R1100	–31.0	**E1196**	**58.9**
R1134	**–44.1**	**E1209**	**61.1**
K1172	–31.7	E1210	39.8
R1175	–34.4	E1238	33.8
R1222	–33.0	D1246	36.7
K1228	–35.9	D1297	33.4
R1240	–35.0	E1303	32.0
R1245	–36.4		
K1250	**–59.3**		
K1251	**–47.3**		
K1257	–38.6		
R1282	**–33.0**		

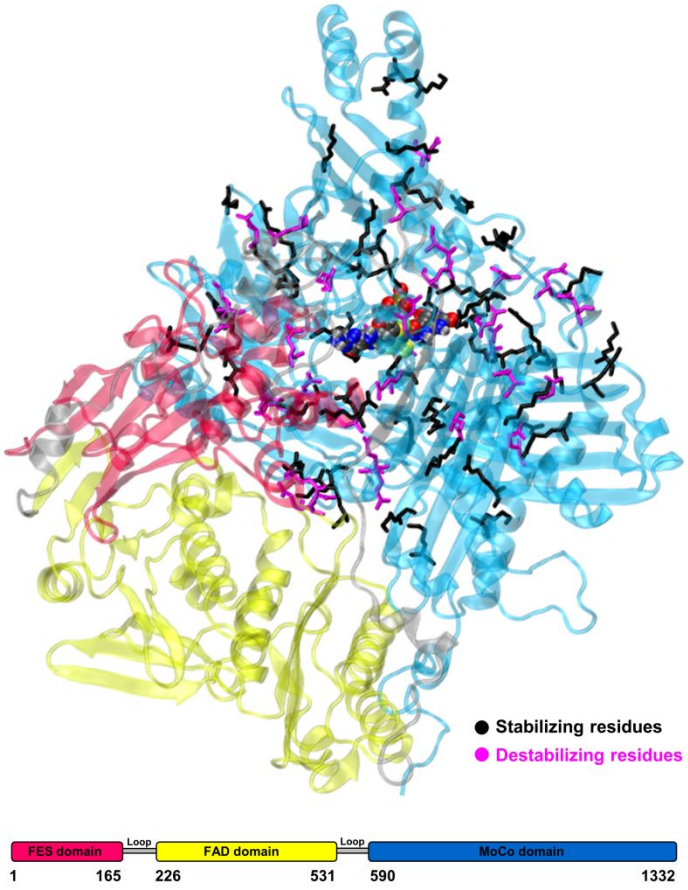

[1] Residues in bold text have significant contributions. Contributions with $|E_{NB}|$ ≥ 30 kcal mol^{-1} are listed in the table.

8. Binding Affinities

Table S4. Binding enthalpies (kcal mol^{-1}) between the XO and oxipurinol calculated via the MM/GBSA approaches.

GBSA components	**XO–OXI**			
	Replicate 1	Replicate 2	Replicate 3	The mean values
E_{VdW}	–23.1	–23.0	–23.6	–23.24
E_{EL}	–38.6	–32.2	–35.3	–35.36
E_{GB}	38.4	34.2	38.4	37.01
E_{SURF}	–2.9	–2.9	–2.9	–2.92
ΔH_{gas}	–61.7	–55.2	–58.9	–58.6
ΔH_{solv}	35.5	31.2	35.6	34.1
ΔH_{bind} ± (Std. Dev.)	–26.2 ± 2.1	–24.0 ± 2.2	–23.3 ± 2.3	–24.5 ± 2.2

GBSA components	**XO–OXI^{T-2}**			
	Replicate 1	Replicate 2	Replicate 3	The mean values
E_{VdW}	–24.2	–24.0	–23.5	–23.9
E_{EL}	–31.0	–27.6	–32.5	–30.4
E_{GB}	31.4	30.3	32.5	31.4
E_{SURF}	–3.0	–2.9	–2.9	–2.9
ΔH_{gas}	–55.2	–51.6	–56.0	–54.3
ΔH_{solv}	28.4	27.4	29.6	28.5
ΔH_{bind} ± (Std. Dev.)	–26.9 ± 2.0	–24.2 ± 2.4	–26.4 ± 2.6	–25.8 ± 2.3

9. QM/MM interaction Energies ($IE_{QM/MM}$)

Table S5. Calculated components of the QM/MM interaction energies ($IE_{QM/MM}$).

System	$\boldsymbol{E_{QM}}$ (kcal mol^{-1})	$\boldsymbol{E_{MM}}$ (kcal mol^{-1})	$\boldsymbol{IE_{QM/MM}}$ (kcal mol^{-1})
XO–OXI	–58.9	–61.1	–120.0
XO–OXI^{T-2}	–84.2	–40.0	–124.2

10. Electron Localization Functions (ELF)

Table S6. Results of the ELF populations (for the atoms in red color) in the critical structures during the XO–OXI complexation.

Basin	Electron population (e^-)		
	Reactant	Approx. TS	Product
V(N8)	2.9	–	–
V(Mo,N8)	–	–	3.1
V(Mo,N8,C)	–	2.7	–
V(O)	–	–	2.3/2.1
V(Mo,O)	5.8	2.9	–
V(O,H)	1.8	1.7	1.8
V(Mo,O,H)	–	3.1	–
V(O,Hε)	–	–	1.8
V(O,Hε,Oε1)	–	1.7	–
V(Oε1)	2.0/2.0	2.6/2.9	2.7/2.7
V(Oε1,Hε)	1.8	0.6	–
V(Oε2)	2.5/2.8	2.5/2.7	2.5/3.0
V(N9)	1.3	1.3	0.7
V(N9,H9)	2.2	2.3	3.0

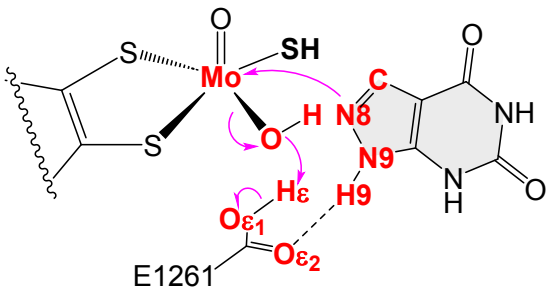

11. Non-covalent Interactions (NCI)

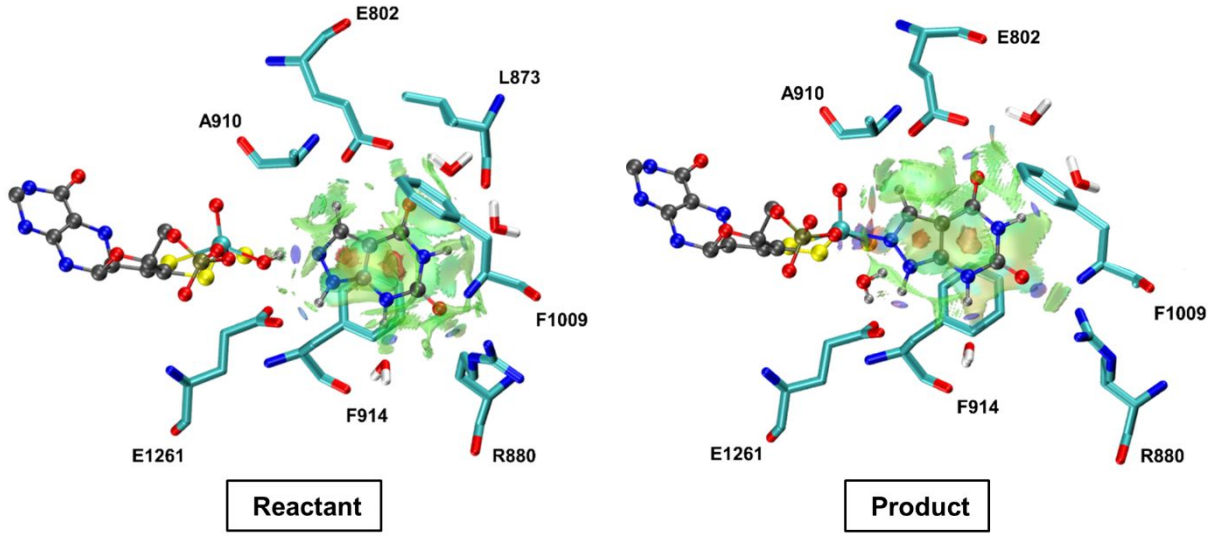

Amino acid	Reactant	Product
E802	✓	✓
L873	✓	–
R880	✓	✓
A910	✓	–
F914	✓	✓
F1009	✓	✓
A1078	–	✓
A1079	–	✓
E1261	✓	✓

Figure S16. Plots of the NCIs between the oxipurinol and the surrounding residues in the reactant and product of the XO–OXI complexation. The MoCo and oxipurinol are illustrated in the ball-and-sticks, while the amino acids and water molecules are in the sticks with different color codes. Residues A1078 and A1079 has non-covalent interactions with the product but are not presented in the figure for more clarity.

12. Mutagenesis Studies *vs.* the Non-bonded Interaction

Table S7. Experimental mutagenesis studies and their effects on XO function versus corresponding non-bonded contributions (E_{NB}) to the MoCo active site calculated via the EDA.

Effect on XO function	Exp. Mutagenesis[1]	E_{NB} (kcal mol^{-1})
Complete loss of function	E802V	–12.3
	R880Q/R880G/R880V	–79.5
	E1261A	N/A [2]
Partial or total loss of function	R149C	–70.8
	G799S	–10.7
	H884Y	–12.9
	N887K	–9.2
	R912W	–155.8
	A1079T	–17.8
Low XO activity[3] (hypouricemia)	R228T	–18.6
	R606Q	–36.1
	K721X	–22.5
	R824X	–38.2
	R1282X	–25.4
High XO activity[3] (hyperuricemia)	I702V	4.3
	H1220R	2.7
	T909M	3.2

[1] Corresponding references for the mutations are given in the manuscript.
[2] E1261 is included in the active site for the EDA. Thus, it has no non-covalent contribution to the active site.
[3] Clinical studies on the mutagenesis of XO, in which either the mutations led to xanthinuria or hyperuricemia.

13. Tautomer-2 (OXI^{T-2})

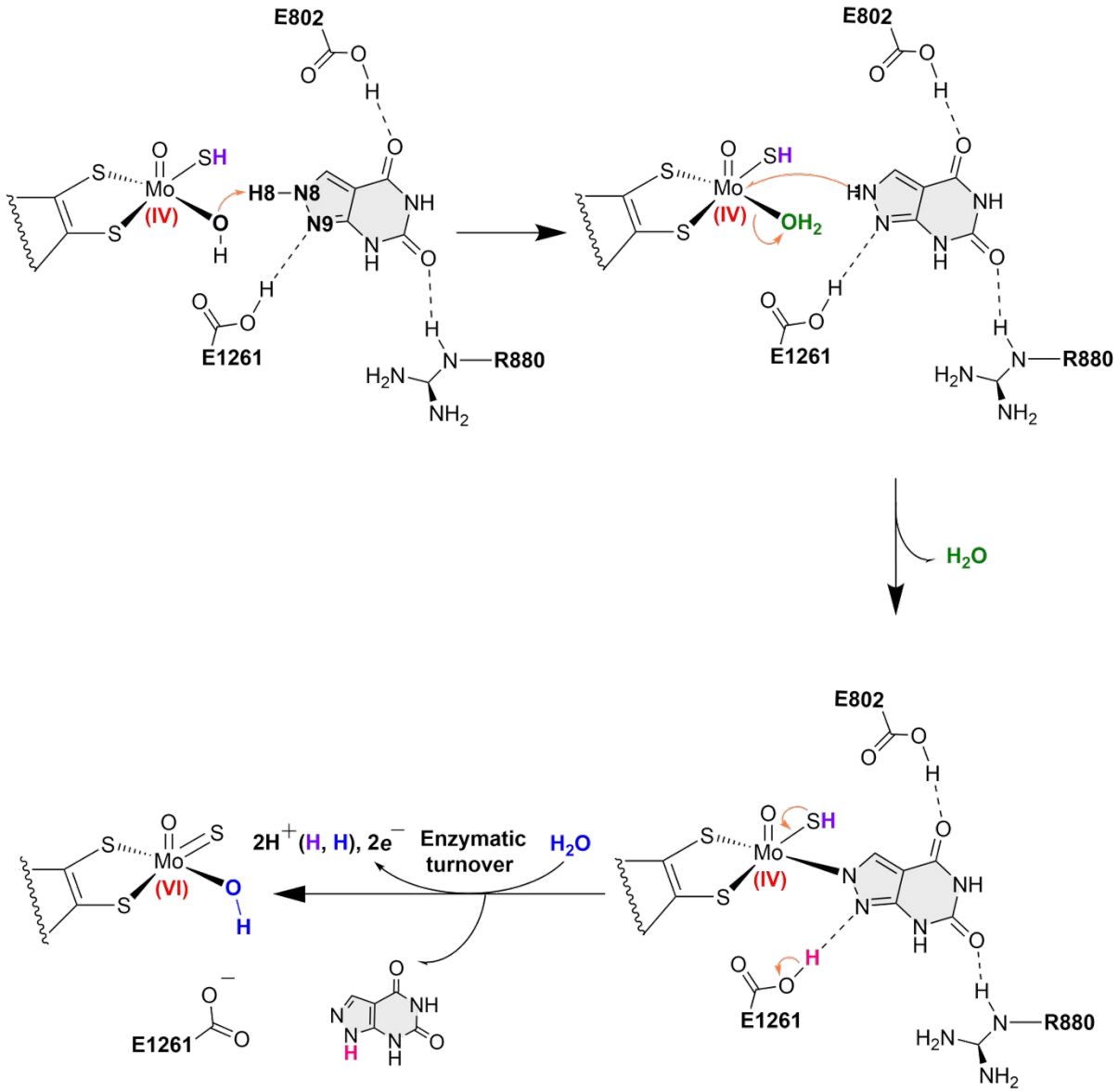

Figure S17. Studied mechanism for the catalytic inhibition of XO by OXI^{T-2}.

The proposed mechanism for OXI^{T-2} involves a proton transfer from the N8 nitrogen of this tautomer to the OH ligand of MoCo, forming an OH_2 ligand. This ligand is then replaced by the N8 of oxipurinol, leading to the MoCo–OXI^{T-2} complexation (see animation in the SI). In the final step, the complex is dissociated by a nucleophilic attack from a hydroxide ion, resulting in the re-oxidation of the molybdenum to its original oxidation state.

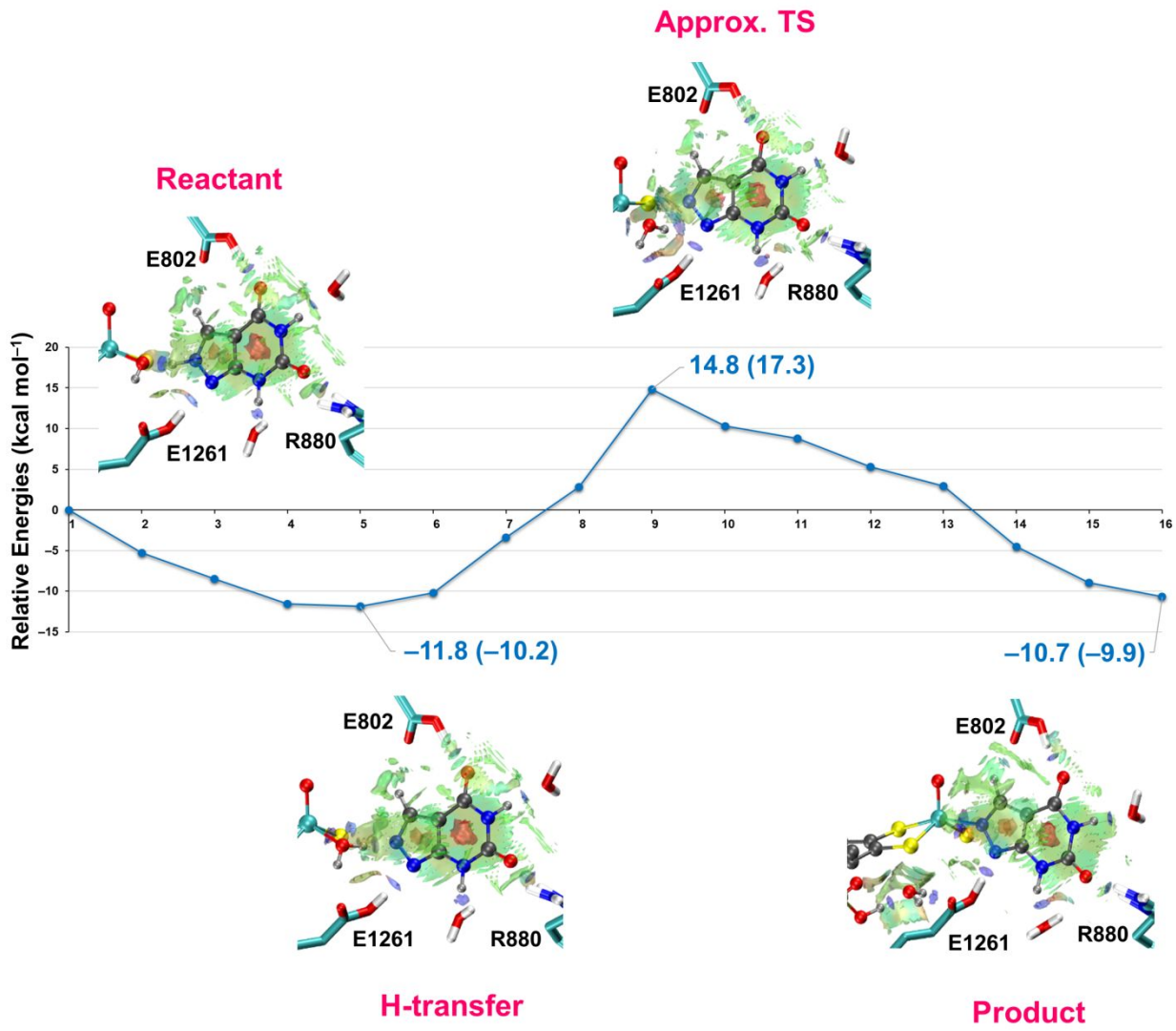

Figure S18. **(A)** The minimum energy path for the catalytic inhibition of XO by OXI^{T-2} modeled via the QSM. The QM/MM optimization energies (kcal mol^{-1}) are calculated at the ωB97X-D/def2-SVP level of theory with AMBER ff14SB force field. The values in parenthesis correspond to the Gibbs free energies obtained from the vibrational analysis using the Eyringpy. The NCI plots between the critical structures and the surrounding residues are also provided.

The XO–OXI^{T-2} reaction is exergonic (ΔE_{react} = –10.7 kcal mol^{-1} and ΔG_{react} = –9.9 kcal mol^{-1}). It involves a spontaneous proton transfer from N8 of OXI^{T-2} to the hydroxyl ligand of MoCo (Mo–OH…H8…N8) resulting in a more stable structure (bead 5) with a stability increase of 11.8(10.2) kcal mol^{-1}. The energy barrier to reach the approximate TS of XO–OXI^{T-2} is 14.8(17.3) kcal mol^{-1} as the Mo…H_2O bond cleaves and the Mo…N8 bond forms. Calculated result of the backward barrier for this form is 25.5(27.2) kcal mol^{-1}, which is in good agreement with the experimental activation energy values for the spontaneous reactivation process ($\Delta G^{\ddagger}_{react}$ = 27 kcal mol^{-1} for bovine XO).

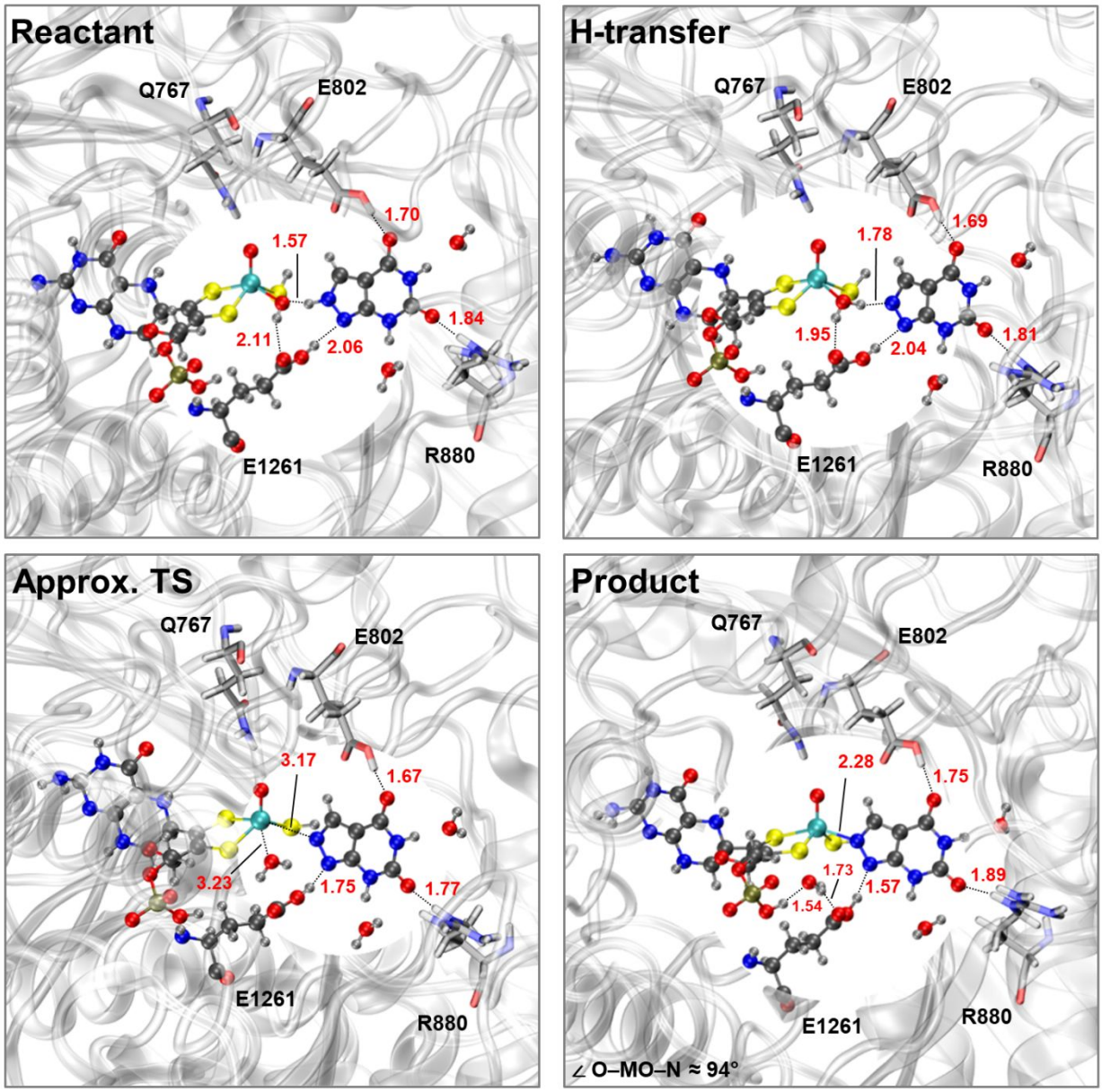

Figure S19. The optimized geometries of the critical structures of the catalytic inhibition of XO by OXI^{T-2}. Values of the selected distances are in angstrom. The MoCo, E1261, and oxipurinol are shown in the ball-and-sticks, while the amino acids of the binding pocket are shown in the sticks. The QM/MM-optimized O–Mo–N angle and Mo–N distance for the product are 94° and 2.28 Å, which agrees with the experimental values of 94.97° and 2.28 Å in the referenced PDB.

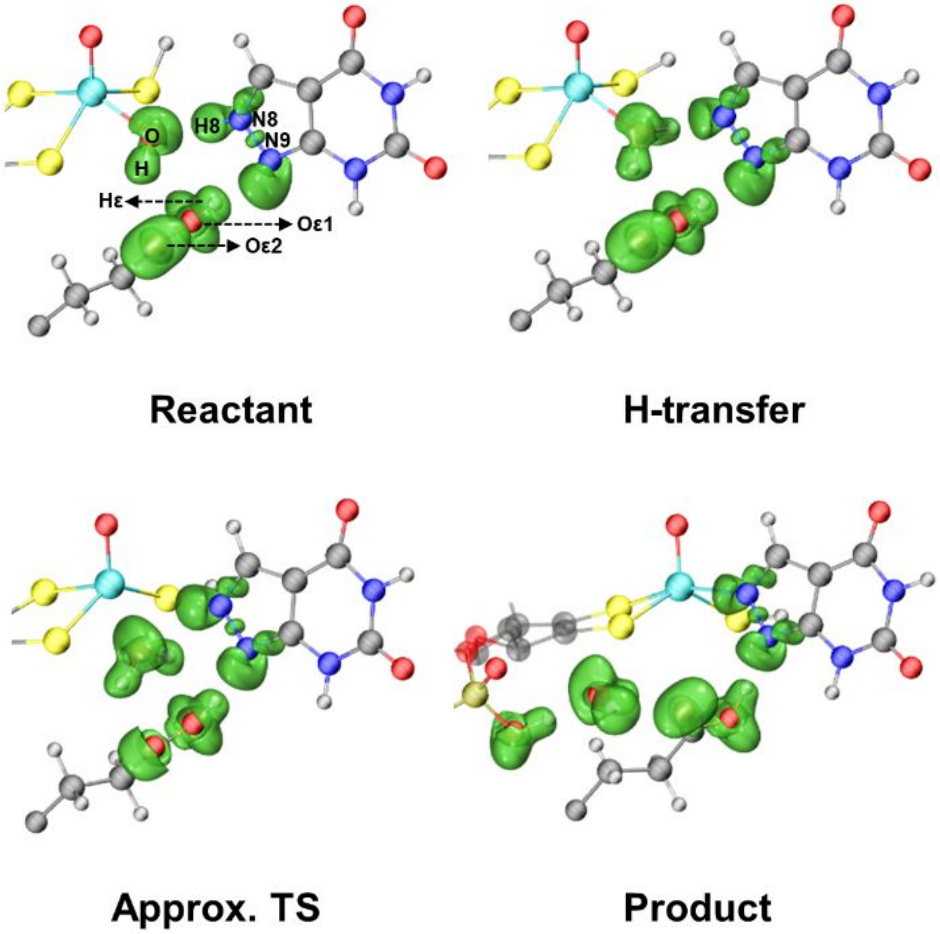

Basin	Electron population (e^-)			
	Reactant	H-transfer	Approx. TS	Product
V(N8)	1.6	3.0	–	–
V(N8,H8)	1.5	–	–	–
V(Mo,N8)	–	–	–	2.9
V(Mo,N8,C)	–	–	3.0	–
V(O)	–	–	2.3	2.0/2.3
V(Mo,O)	4.6	2.4	–	–
V(O,H)	1.7	1.8	1.7	1.7
V(Mo,O,H)	–	–	2.1	–
V(O,H8)	–	1.9	1.8	1.8
V(Oε1)	4.1	4.0	4.0	4.0
V(Oε1,Hε)	1.9	1.9	1.9	2.0
V(Oε2)	2.5/2.7	2.6/2.7	2.7/2.6	2.7/2.6

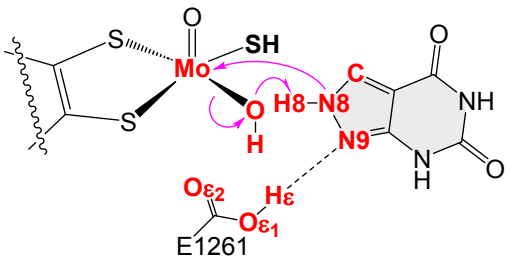

Figure S20. The ELF basins and populations for the critical structures along the XO–OXI^{T-2} inhibition reaction pathway.

The depiction of the ELF basins indicate the formation of V(O,H8) disynaptic basin (1.9 e^-) in the H-transfer step. It is worth mentioning that the electron population for V(N9,H9) in the reactant of XO–OXI (the major tautomer) is 2.2 e^-, while this value for V(N8,H8) in XO–OXI^{T-2} is 1.5 e^-. This 0.7 e^- difference, combined with the NCI surfaces detected between the H8 of OXI^{T-2} and the hydroxyl ligand of MoCo (see **Figure S18**), as well as the short Mo–O...H8–N8 distance of 1.57 Å (see **Figure S19**), may provide an explanation for the spontaneous proton transfer. In the approximate TS, the formation of trisynaptic basins, V(Mo,N8,C) and V(Mo,O,H), with population values of 3.0 e^- and 2.1 e^-, respectively, suggests the initiation of Mo–N8 formation and the cleavage of Mo–H_2O bonds. Eventually, V(Mo–N8) disynaptic basin with a population of 1.9 e^- forms in the product due to complexation.